CSIRO PUBLISHING

Australian Journal of Physics

Volume 51, 1998

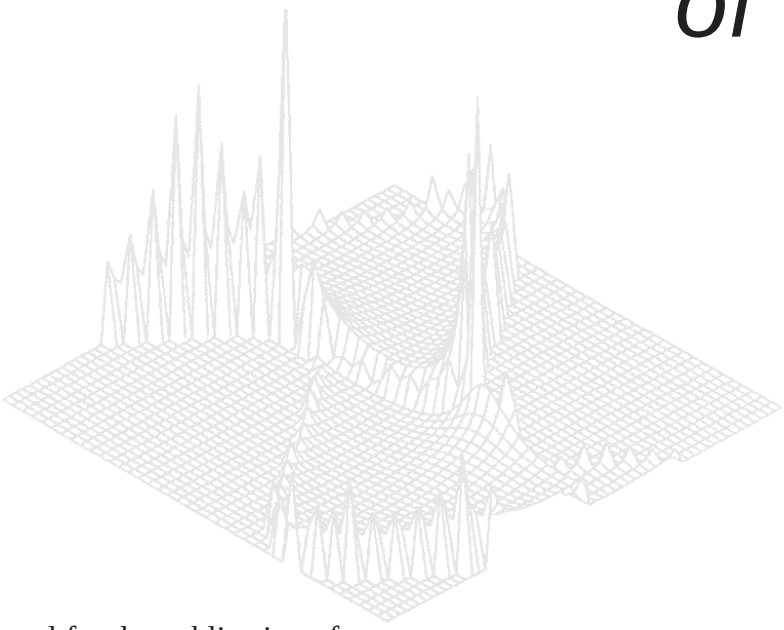

A journal for the publication of
original research in all branches of physics

www.publish.csiro.au/journals/ajp

All enquiries and manuscripts should be directed to
Australian Journal of Physics
CSIRO PUBLISHING
PO Box 1139 (150 Oxford St)
Collingwood Telephone: 61 3 9662 7626
Vic. 3066 Facsimile: 61 3 9662 7611
Australia Email: peter.robertson@publish.csiro.au

Published by **CSIRO** PUBLISHING
for CSIRO and the
Australian Academy of Science

Aust. J. Phys., 1998, **51**, 971–1010

A VLA Survey of Rich Clusters of Galaxies*
IV. An Analysis of the Results

O. B. Slee,[A] *A. L. Roy*[B] *and H. Andernach*[C]

[A] Australia Telescope National Facility, CSIRO,
PO Box 76, Epping, NSW 2121, Australia.
[B] National Radio Astronomy Observatory, PO Box 0, Socorro, New Mexico, USA.
[C] Depto. de Astronomìa, IFUG, Apdo. Postal 144, Guanajuato, Mexico.

Abstract

We present a detailed analysis of the results of a two-frequency VLA survey with scaled arrays of 60 fields near 58 Abell clusters. The sample of sources is complete to a flux density of 2·0 mJy at 1·5 GHz, from which we chose two sub-samples of radio galaxies from clusters that had been surveyed completely out to 0·24, and 0·51 times the Abell radius $R_{\rm A}$ respectively. The following conclusions are drawn from these samples: (i) The sources are strongly concentrated towards their cluster centres, showing a power-law variation of surface density with radius, with an exponent of $\sim -1{\cdot}6$. Each cluster contains an average of two radio galaxies. (ii) The ratios of flux density and surface brightness in the lobes of cluster and background doubles are very similar, as are their spectral indices; the ratios of component area are significantly different. (iii) The lobes of cluster doubles have spectra that steepen with radio power, but a less significant relationship is found between spectral index and surface brightness. (iv) Relationships are found between source area and radio power, optical luminosity and $r/R_{\rm A}$, spectral index and $r/R_{\rm A}$, and between radio power and optical luminosity. (v) We define three polarisation classes on the basis of the presence or absence of observable polarisation at 4·9 and 1·5 GHz; the physical parameters vary systematically across the classes. (vi) Depolarisation in sources that are partially polarised at both frequencies (Class I) is predominantly caused by tangled fields; sources that are polarised at only the higher frequency (Class II) or at neither frequency (Class III) are depolarised by a combination of tangled fields and differential Faraday rotation. The rms dispersion in the scale size of the tangled fields within the radio plasma is ∼5 kpc. (vii) Differential Faraday depolarisation in Classes I and II suggests that thermal electrons are entrained in the radio plasma with densities in the range $1{\cdot}1$–$2{\cdot}3\times10^{-4}$ cm^{-3}. (viii) The magnetic fields in Class I doubles (with minimum Faraday rotation) favour directions predominantly parallel to the major axis of the double. (ix) The univariate fractional luminosity function suggests that an early-type cluster galaxy with $M_{\rm R} \leq -21{\cdot}0$ has a probability of ∼0·02 of creating a radio source with $P_{1{\cdot}5} \leq 10^{24{\cdot}9}$ W Hz^{-1}. (x) The integrated bivariate fractional luminosity function shows that higher luminosity cluster galaxies are more likely to form radio sources, although in each bin of absolute magnitude the fraction of radio sources decreases with increasing radio power. (xi) The average lifetime of a cluster source of $\sim 2\times10^6$ yr is consistent with the travel-time of the plasma at ∼3000 km s^{-1} from a once-only acceleration site near the centre of the host galaxy. (xii) The confinement of the radio lobes can be easily accomplished by the static pressure of the hot intra-cluster gas and/or ram pressure generated by the passage of the galaxy through the gas. (xiii) Radio powers of cluster sources and optical luminosities of their hosts are both independently correlated with cluster X-ray luminosity. This suggests that radio power is maintained by the confining pressure of the hot gas, but the cause of the

* Paper I, *Aust. J. Phys.*, 1989, **42**, 633; Paper II, *Aust. J. Phys.*, 1994, **47**, 145; Paper III, *Aust. J. Phys.*, 1996, **49**, 977.

 10.1071/PH97087 0004-9506/98/060971$15.00

optical correlation is unknown. (xiv) Finally, core powers in cluster radio galaxies are of the same order as those in non-cluster sources, indicating that the hot intra-cluster gas does not provide an extra fuel supply for the nuclear engine.

1. Introduction

Radio surveys of large samples of galaxy clusters with good angular resolution are needed to establish whether their radio galaxies differ from those identified in complete surveys of sky areas that do not contain obvious nearby clusters. One needs to first separate the cluster sources from those in the background before proceeding to measure cluster source parameters such as:

(1) the cluster radio luminosity function;
(2) the radial variation in projected cluster source density from the cluster centroid;
(3) the spectral index distribution of cluster sources;
(4) the optical identification fraction and its variation with flux density;
(5) the influence of the hot intra-cluster gas on radio power and morphology;
(6) the polarised fraction in cluster sources and whether its position angle is related to the major axis of a resolved source;
(7) the morphology and absolute magnitudes of host galaxies; and
(8) the core powers of cluster sources versus those in the general field.

A number of multi-cluster surveys with arcmin resolution have been published, e.g. Fomalont and Rogstad (1966), Riley (1975), McHardy (1978), Mills and Hoskins (1977), Owen *et al.* (1982), Slee *et al.* (1983), Slee and Siegman (1983), and Andernach *et al.* (1988 and references therein). While these low-resolution surveys attempted to establish the cluster radio luminosity function, and the degree of concentration of cluster sources to the cluster centroid, they all suffered from the inability to resolve cluster from background sources, make positive optical identifications and, because the surveys were generally made at a single frequency, establish the spectra of the weaker sources.

The advent of the synthesis telescope resulted in at least an order of magnitude improvement in both sensitivity and angular resolution, although there were few multi-cluster surveys that attempted to detect all the sources in the complete cluster down to the flux density limit and could therefore be used for convincing statistical conclusions about cluster-source parameters. There were even fewer surveys that utilised scaled arrays to derive accurate spectral indices for the sources. As far as the authors are aware, such complete multi-cluster surveys are those of Jaffe and Perola (1975), Reynolds (1986), Ledlow and Owen (1995*a* and references therein) and Slee *et al.* (1989, 1994*a*, 1996). These data are capable of providing solutions to the problems raised by the low-resolution, low-sensitivity data described above. In addition, synthesis telescopes in their higher-resolution configurations can often reveal the detailed morphology of a cluster source, which is often influenced by the thermal pressure of the hot intra-cluster gas.

Between 1981 and 1985 the Very Large Array (VLA) was used to survey 60 fields near 58 Abell clusters of galaxies (Abell 1958; Abell *et al.* 1989). The results have been published in Slee *et al.* (1989, Paper I; 1994*a*, Paper II; 1996, Paper III). The fields were surveyed using the snapshot mode in the scaled C and D configurations at 1·5 GHz and 4·9 GHz, respectively; five fields were mapped

at 1·5 GHz only. In addition, a few of the clusters were observed in the scaled B and C configurations. In the C/D configurations, the angular resolution was ∼14 arcsec in right ascension, but was up to a factor of two larger in declination for the southernmost clusters at −30°. In the scaled B/C configurations, the maximum resolution was ∼4 arcsec.

The VLA fields were centred on strong steep-spectrum sources with spectral indices $\alpha \leq -0{\cdot}9$ [defined by $S(\nu) \propto (\nu/\nu_0)^{\alpha}$] discovered in an earlier low-resolution survey with the Culgoora circular array at 80 and 160 MHz (Slee and Siegman 1983). The sample is not complete, either out to a distance limit or in terms of richness of galaxies and cluster morphology. Nevertheless, the sample is believed to be representative of the cluster population, as it includes clusters with the full range of richness and distance.

A preliminary analysis of some observed and intrinsic radio parameters was made in Section 5 of Paper I. Section 6 of Paper II treated in some detail the distributions in flux density, emitted power and linear diameter of the sources with 1·5 GHz flux density ≥20 mJy. In this paper we first define the criteria for cluster membership and then examine the relationships between a number of radio, optical and X-ray parameters. We treat the complete sample of 765 radio sources from Papers II and III with flux densities ≥1 mJy at 1·5 GHz, which fell within the FWHP circle (30 arcmin) on the 1·5-GHz maps.

Throughout this paper computations of absolute magnitude, emitted power and linear dimensions use $H_0 = 75\ \mathrm{km\,s^{-1}\,Mpc^{-1}}$ and $q_0 = 0{\cdot}5$. We use $S_{1\cdot5}$ and $S_{4\cdot9}$ to denote flux densities at 1·5 and 4·9 GHz, respectively, and $P_{1\cdot5}$ and $P_{4\cdot9}$ to represent the corresponding emitted radio powers.

2. Identification Fractions for the Complete Sample

(2a) Flux-density Distribution at 1·5 GHz

Fig. 1 shows our differential source count of $\log(\Delta N/\mathrm{sr})$ versus $\log(S_{1\cdot5}/\mathrm{mJy})$ from the complete sample of 765 sources as described in Section 1. The dashed curve is the polynomial fit by Wall (1994) to several sets of data at 1·41 GHz from completely surveyed samples of field sources. Our source counts fall away sharply in the lowest two flux density bins [all of width 0·30 in $\log(S_{1\cdot5}/\mathrm{mJy})$]; our count is also lower by ∼0·25 in the log for the third lowest bin [centred on $\log(S_{1\cdot5}/\mathrm{mJy}) = 0{\cdot}4460$], but the three data sets in the range $0 < \log(S_{1\cdot41}/\mathrm{mJy}) < 1$ contributing to Wall's fit all fall below his curve by ∼0·3 in the log. We therefore accept that our source count in the bin $2{\cdot}0 \leq \mathrm{S}_{1\cdot5} \leq 3{\cdot}9$ mJy is essentially complete. Accordingly, from now on we define our complete flux-density-limited sample as those 662 sources with $S_{1\cdot5} \geq 2{\cdot}0$ mJy.

Our counts at $S_{1\cdot5} \geq 100$ mJy exceed those of the field sources by a factor of up to six, but this is not surprising as these fields were chosen because of the presence of strong 80 and 160 MHz sources, and so are not counts from survey centres chosen at random in the sky. The major reason for the rapid decline in detections for $S_{1\cdot5} < 2{\cdot}0$ mJy is the presence of uncleaned side lobes of the stronger sources in each field. The dynamic ranges of the whole-field maps (published in Paper I) varied from 50 : 1 to 400 : 1 with an average of 226 : 1, where the dynamic range is here defined as the ratio of the peak brightness

to the lowest brightness contour on the map. Each map was assessed for its likely side-lobe level, taking into account the brightest source, the formal rms measurement in a large area clear of obvious sources and evidence of response patterns with symmetry about strong sources. We made no systematic attempt to catalogue all sources above a multiple of the rms, but used our subjective assessment of the reality of a weak source. As a result, we rarely catalogued a response with peak brightness <10 rms and, if particularly bright sources were present, <20 rms. From Fig. 1, many of the rejected responses below 2·0 mJy must be real sources, but our conservative analysis procedure has resulted in defining a legitimate lower limit to the survey.

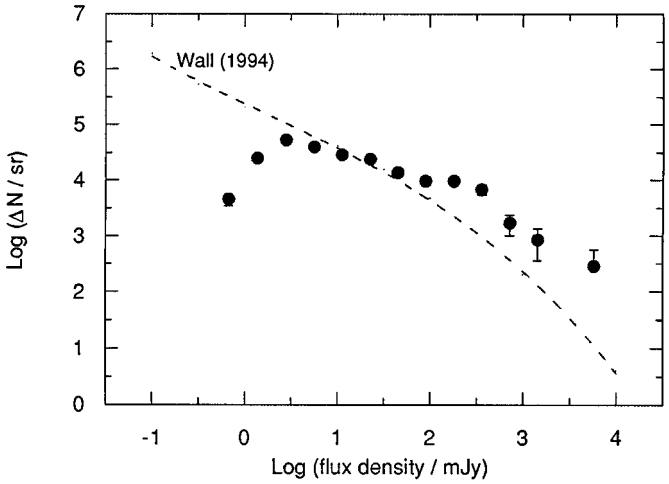

Fig. 1. Differential log$N$–log$S$ distribution for the 765 sources within the FWHP primary beam at 1·5 GHz. The dashed line is the differential log$N$–log$S$ curve for whole-sky surveys from Wall (1994).

This complete sample includes 254 sources identified with galaxies and 51 with star-like (St) images. Of the 254 galaxies, 121 are regarded as cluster members, because they are within one Abell radius of the cluster centroid and satisfy the redshift and/or brightness criteria to be discussed in detail in Section 2d. The subset of cluster galaxies is not to be regarded as complete in the sense that it has been drawn from clusters that have been fully surveyed out to an Abell radius; such statistically complete samples will be extracted from the above numbers in Section 2d.

(2b) Identifying Sources with Galaxies

The identification criteria were discussed in detail in Papers II and III. Generally, the optical image fell within 10 arcsec of the radio centroid, although exceptions were made for some extended sources, where structural features suggested that a more distant galaxy would be the more appropriate identification. We consider here only identifications from the complete sample as defined in Section 2a.

Fig. 2 shows the percentage identification of radio sources with galaxy images as a function of flux density. Here, we did not distinguish between cluster and non-cluster galaxies. The identification rate rises from ∼28% at the lowest flux densities to ∼80% at the highest.

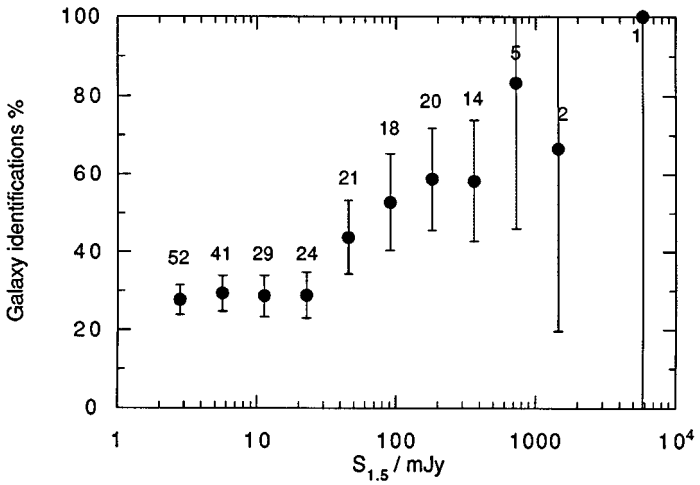

Fig. 2. Distribution with flux density of identification fractions for sources identified with galaxy images on survey plates. The number N of identified sources contributing is printed above each point. The error bars are proportional to $\pm\sqrt{N}$.

The probability that an unrelated galaxy will fall by chance within the circle about the source centroid defined by the suggested identification depends strongly on the magnitude of the galaxy and its angular distance from the radio centroid. For example, we estimated the expected number of spurious associations for the 41 identifications with $4{\cdot}0 \leq S_{1{\cdot}5} \leq 7{\cdot}9$ mJy of Fig. 2. We used the differential galaxy densities of Tyson and Jarvis (1979) at $|b| = 47°$ (the median Galactic latitude of our clusters) and the median angular off-set in each one-magnitude brightness range $14{\cdot}0 < m_J < 23{\cdot}0$ to compute the most likely number of chance associations in each one-magnitude interval. For the fields around the 140 radio sources contributing to identifications in this bin, the total expectation was $7{\cdot}7$ galaxies, but $6{\cdot}4$ of these can be attributed to the faintest magnitude range $22{\cdot}0 < m_J < 23{\cdot}0$, in which we identified only four radio sources. This suggests that the identifications for these faintest objects are not reliable. Over the remainder of the brightness range, the number of identifications exceeds the expected number of spurious identifications by at least 20/1.

We adopted a similar approach with the 121 cluster galaxy identifications from 662 radio sources in the complete sample as defined in Section 2*a*. These were the radio sources identified with galaxies satisfying the cluster identification criteria of Section 2*d* and with $r/R_{\rm A} \leq 1{\cdot}0$, i.e. with projected distance from the cluster centre less than one Abell radius. The 58 clusters from which they were chosen were often not completely surveyed out to the Abell radius. In this case we used the differential counts in the range $13{\cdot}0 < m_J < 22{\cdot}0$ and the median angular off-set in each one-magnitude range to compute the expected number of spurious identifications in each one-magnitude range. The total expectation was $4{\cdot}3$ galaxies, with most ($2{\cdot}9$) occurring in the brightness range $21{\cdot}0 < m_J < 22{\cdot}0$, in which we suggested three identifications. Over the rest of the brightness range the number of identifications exceeds the expected number of chance associations by at least 26/1 and so we have a high degree of confidence in this range.

(2c) Star-like Identifications

The search area for star-like (St) identifications was a circle on the survey plates with a radius of 10 arcsec; sharp images were accepted as St identifications in the brightness range $11{\cdot}9 \leq m_J \leq 21{\cdot}0$. Fainter objects are difficult to classify without additional colour and spectroscopic data, but Tyson and Jarvis (1979) showed that the surface density of galaxies exceeds that of stars for $m_J \geq 22{\cdot}0$. We classified images fainter than $m_J = 21{\cdot}0$ as galaxies but, in any case, only three such images were detected near radio centroids. Fig. 3 shows the percentage identification rate for St identifications over the flux-density range of the complete sample. The identification rate is $\sim 7{\cdot}5\%$ and is relatively independent of flux density.

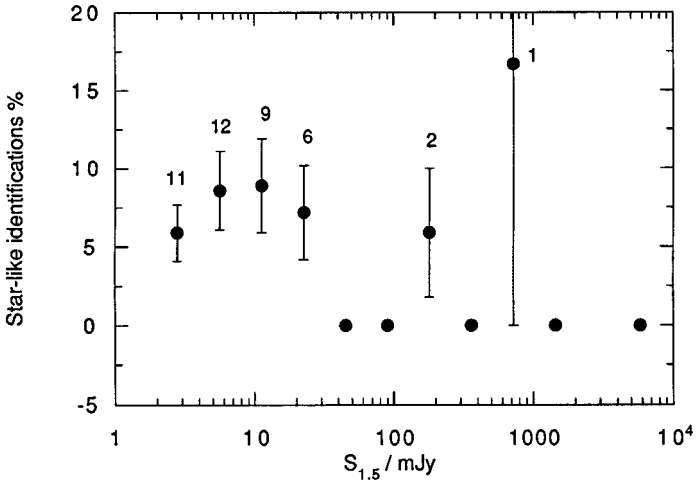

Fig. 3. Distribution with flux density of identification fractions for sources identified with star-like images on survey plates. The number N of identified sources contributing is printed above each point. The error bars are proportional to $\pm\sqrt{N}$.

To estimate the number of chance intruders in the St identifications, we adopted the differential star densities of Bahcall and Soneira (1980) in the region $|b| = 50°$, $|l| = 90°$, which lies near the median value for our radio fields. We found the expected star numbers in each one-magnitude brightness range for $11{\cdot}0 < m_J < 21{\cdot}0$, using the median angular offset for the identifications in each brightness interval. For this we estimate $18{\cdot}3 \pm 2{\cdot}7$ spurious St identifications, which is about half the observed number of 43 St identifications in the fields around 662 radio sources in the complete sample. We repeated the calculation for the 15 St identifications that fell within 5 arcsec of the radio centroid, and therefore even more likely to be correct identifications for relatively unresolved radio sources. This time we utilised their individual offsets and optical magnitudes to compute the probability of a stellar intruder. The number of expected stars from the 662 radio source fields was $8{\cdot}85 \pm 1{\cdot}33$, confirming the excess of $\sim 2:1$ for the 15 observed St identifications. The difference of a factor of ~ 2 is maintained over the complete magnitude range of the St identifications. The excess can almost certainly be attributed to QSOs, because the probability of finding a QSO

within 10 arcsec of a radio-source centroid is high compared to that in a field chosen at random. Indeed, the few investigations of this problem (e.g. Kron *et al.* 1985; Windhorst *et al.* 1985) suggest that up to 20% of radio sources with $S_{1\cdot4} \geq 1$ mJy are probably QSOs although, in most cases, the QSO morphology was assigned on the basis of a star-like image and a colour index typical of QSO. In our VLA sample, if half the St identifications are really QSOs, they constitute only 10% of the total number of identifications; this includes the four catalogued quasars in our sample. Our lower QSO identification fraction is almost certainly due to the brightness limit of $m_J \sim 21{\cdot}0$ for our St images, compared with a limit of $m_J \sim 23{\cdot}0$ for the work quoted above.

A few of the excess St identifications may be true stars, especially if the radio source is not well resolved, has a low (<10 mJy) 1·5-GHz flux density and a centroid position within 2 arcsec of the optical image. Three identifications in this category are those associated with the sources A86__7, A1189__3 and A2670__13. A1189__3 is 2 arcsec from a bright ($m_J = 11{\cdot}9$) stellar image (GSC 00263–00366) which, in 662 radio source fields, has a chance probability of 0·005. Ryan (1989) describes this star as a cool (B-V = 0·62) dwarf of high proper motion, but a subsequent spectrum (S. G. Ryan, private communication) is that of a normal inactive star. The other two objects, A86__7 and A2670__13, have chance probabilities, in 662 radio fields, of 0·08 and 0·18 respectively, but no spectroscopic observations have yet been made of them.

(2d) Complete Samples of Cluster Sources

We outline in this subsection how one can define a sample of radio sources that have a high probability of cluster membership. Our criteria for the selection of a cluster source are that:

(i) the source has $S_{1\cdot5} \geq 2{\cdot}0$ mJy and lies within the FWHP of the primary beam;
(ii) the radio source is identified with a galaxy with a measured redshift within twice the velocity dispersion of galaxies in the cluster; the cluster radial velocity dispersion was obtained from the redshift reference in Table 1 of Paper III, but if the cluster's redshift came from the m_{10}–z relationship, a representative value of 800 km s^{-1} was assumed for the cluster's radial velocity dispersion;
(iii) the galaxy has no measured redshift but, if using the measured or estimated redshift of the cluster, its absolute red magnitude would be $M_{\rm R} \leq -21{\cdot}0$; and
(iv) sources in empty fields or identified with galaxies with $M_{\rm R} > -21{\cdot}0$ (assuming the cluster redshift) are considered to be at distances well beyond the cluster.

Strictly, some of the galaxy identifications that satisfy the above condition could be foreground objects, but an examination of their radio and optical flux density distributions can provide additional information on their background versus foreground status. Galaxies with $M_{\rm R} \leq -21{\cdot}0$ have medians of $S_{1\cdot5} = 41{\cdot}7$ mJy and $m_{\rm R} = 15{\cdot}9$ mag; galaxies with $M_{\rm R} > -21{\cdot}0$ have medians of $S_{1\cdot5} = 6{\cdot}6$ mJy and $m_{\rm R} = 18{\cdot}3$ mag. Therefore, assuming that the two categories possess similar distributions of emitted radio and optical power and a Euclidean cosmology, the

great majority of the objects that do not satisfy the red luminosity criterion will be at distances $\sim 2 \cdot 75$ times those of the clusters on which they are projected.

First, we must justify the use of $M_{\rm R} = -21 \cdot 0$ as a discriminator between cluster and non-cluster (background) galaxies, since many of our conclusions depend on this characteristic. We choose $M_{\rm R} \leq -21 \cdot 0$ because we find that E/S0 galaxies that are identified with radio sources and that have measured redshifts almost invariably have $M_{\rm R} \leq -21 \cdot 0$ (including K-corrections and Galactic and atmospheric corrections). This is apparent in Fig. 4, which shows the distribution of $M_{\rm R}$ for galaxy identifications with redshifts in our complete sample with $S_{1 \cdot 5} \geq 2 \cdot 0$ mJy and within the FWHP circles on our maps. These galaxies display a sharp cut-off in the distribution at $M_{\rm R} > -21 \cdot 0$.

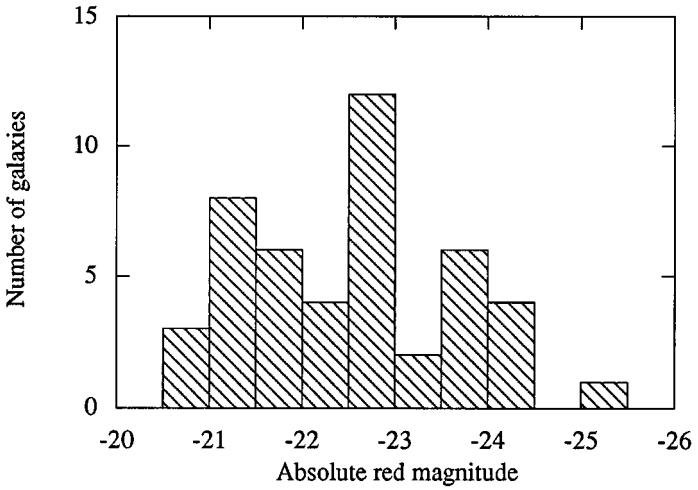

Fig. 4. Distribution with absolute red magnitude (corrected to the rest frame of the cluster) of our cluster sources with individually measured redshifts.

Our magnitude estimates come from the Palomar and SRC Sky Survey plates so it is important to establish the accuracy of our estimates of $M_{\rm R}$. Fortunately, we had 27 identifications (included in Fig. 4) in common with Ledlow and Owen (LO, 1995*b*), who did accurate CCD photometry of these galaxies and converted the measured magnitudes to $M_{\rm R}$ in the rest frames of the 19 clusters involved. The average difference in the common but independent estimates of $M_{\rm R}$ was $\langle \text{Present paper} - \text{LO} \rangle = +0 \cdot 21 \pm 0 \cdot 12$ (standard error). Thus our estimates of $M_{\rm R}$ tend to be slightly fainter than those of the more accurate values of Ledlow and Owen, but the difference is small enough to validate the cut-off in Fig. 4 at $M_{\rm R} = -21 \cdot 0$.

The cut-off in Fig. 4 for radio galaxy identifications is not induced by observational limitations, despite the fact that only 39% of our galaxy identifications have measured redshifts. The median values for $m_{\rm R}$ (corrected for atmospheric extinction) are $14 \cdot 8$ and $16 \cdot 3$ mag. for the galaxies with and without measured redshifts respectively. The difference in the magnitude distributions is significant on a K–W ranking test, but the group without measured redshifts is still bright

enough to provide easily measurable values. The validity of the cut-off is supported by Ledlow and Owen (1995*b*), who used a large complete sample of identified cluster sources with measured redshifts to show that all E/S0 galaxy identifications with $M_{\rm R} \geq -21{\cdot}0$ were background objects. Further confirmation of the cut-off is provided by Sadler *et al.* (1989), who found from a complete flux-limited sample of radio sources identified with nearby (<100 Mpc) E/S0 galaxies that sources with $P_{1{\cdot}5} \geq 10^{21}$ WHz^{-1} (a factor of 10 below the lowest power in our sample) were invariably associated with galaxies having $M_{\rm R} \leq -21{\cdot}0$.

Using the criteria above, we defined two complete samples of radio sources:

(i) clusters surveyed completely out to $r/R_{\rm A} = 0{\cdot}51$;
(ii) clusters surveyed completely out to $r/R_{\rm A} = 0{\cdot}24$,

where $r/R_{\rm A}$ is the projected distance of the source centroid from the cluster centroid expressed as a fraction of the Abell radius.

We defined the second sample in order to include a greater number of clusters in the statistics, although it has the disadvantage that a smaller area of each cluster is surveyed. Necessarily, all the clusters in sample (i) are included in sample (ii). The difference in cluster numbers arises because not all radio fields were centred on the associated cluster centroids; also, the criterion that all samples had to be contained within the FWHP circle on each map had to be satisfied. We minimised errors in $r/R_{\rm A}$ by fitting elliptical Gaussians to the EINSTEIN and ROSAT images available in the public data bases; failing that, we used either the XBACS ROSAT centres of Ebeling *et al.* (1996) or, as a last resort, the optical cluster centres in Abell *et al.* (1989). By this means, we obtained accurate cluster centre positions from which reliable values of $r/R_{\rm A}$ were computed.

Table 1. Identification statistics of complete samples of radio sources

Range Abell radius	Number of clusters	No. of cluster gals. (ident %)	No. non-cluster gals. (ident %)	No. St idents (ident. %)	No. empty fields (%)	Total no. of sources
0 to $\leq 0{\cdot}51$	28	59 (33·5)	26 (14·8)	10 (5·7)	81 (46·0)	176
0 to $\leq 0{\cdot}24$	41	66 (44·3)	22 (14·8)	7 (4·7)	54 (36·2)	149

(2e) Identification Fractions in the Complete Cluster Samples

The identification fractions for the samples selected according to the criteria in Section 2*d* are set out in Table 1. Here, the numbers of sources identified with cluster galaxies, with stars and with empty fields can be legitimately compared because they are drawn from the same areas of sky surrounding the cluster centres. The numbers of galaxies and stars in Table 1 have *not* been corrected for chance associations which, as explained in Sections 2*b* and 2*c*, are negligible.

It is clear from Table 1 that 66·5% of the sources in the sample out to $r/R_{\rm A} \leq 0{\cdot}51$, and 55·7% in the sample out to $r/R_{\rm A} \leq 0{\cdot}24$, are *not* associated with galaxies in the surveyed clusters but with much more distant galaxies or, in some cases, with QSO or Galactic stars. Note that the identification fractions for galaxies (totals of 48·3% and 59·1%) are much higher than the average

corresponding quantities for the complete sample of 662 sources plotted in Fig. 2 as a function of source flux density. This is not surprising because it reflects the concentration of radio galaxies towards the cluster centres, an aspect that will be discussed more quantitatively in the next section. The fractional star-like identifications in Table 1 are consistent with those for the complete sample in Fig. 3.

3. Concentration of Cluster Sources to the Cluster Centre

We have already shown in Section 5 of Paper I that radio sources from this VLA survey are strongly concentrated towards the cluster centres, especially those with $S_{1\cdot5} \geq 20$ mJy. That analysis, however, was restricted because we had no means of distinguishing between cluster members and unrelated background objects except in the statistical sense of using the results of a deep VLA survey of a non-cluster field to compute the expected number of background sources in equal-area circular areas about the cluster centre. From the analysis reported in Sections 2*d* and 2*e*, we are now able to plot the radial distributions of two samples of sources uncontaminated by background objects.

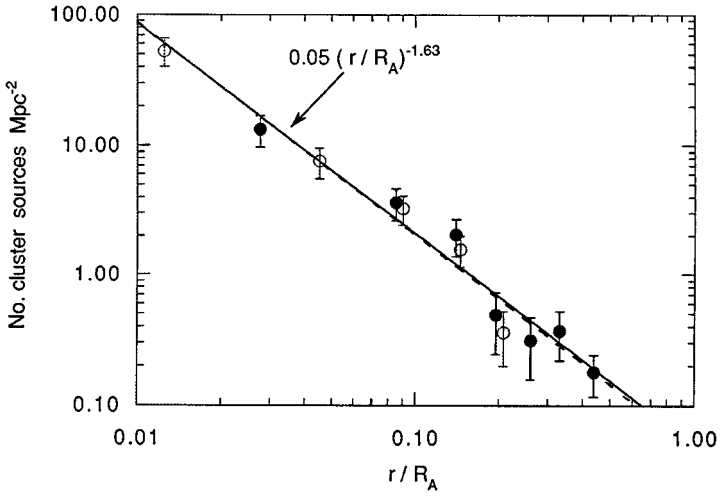

Fig. 5. Radial variation in the surface density of cluster sources. Open circles refer to the sample with $0 \leq r/R_{\rm A} \leq 0{\cdot}24$ and filled circles to the sample with $0 \leq r/R_{\rm A} \leq 0{\cdot}51$. The error bars are equal to $\pm\sqrt{N}$, where N is the number of sources contributing to each point. The power-law fit is to all the data.

We counted cluster sources in annular areas centred on the cluster centroid with spacings at convenient intervals of $r/R_{\rm A}$. The projected cluster area that was surveyed in each annulus was used to find the projected source density Mpc^{-2}. The resulting radial variation in the projected density of cluster sources is shown in Fig. 5; 28 clusters contribute 59 sources to the sample out to $r/R_{\rm A} = 0{\cdot}51$ and 41 clusters provide 65 sources to the sample out to $r/R_{\rm A} = 0{\cdot}24$. The power-law fits to the two samples virtually overlap in Fig. 5, the average regression line giving a variation proportional to $(r/R_{\rm A})^{-1\cdot63}$.

The slope found above for the surface density is steeper than those presented by Andernach and Andreazza (1990). These authors based their analysis on counts of radio sources in annuli around Abell centres from five large-area radio source surveys with much lower angular resolution and sensitivity than the present VLA survey. The shallower decrease in surface density with projected cluster-centre distance found by them may be due to the fact that they include any radio source, regardless of whether it is identified with a cluster galaxy. In addition, their inability to resolve neighbouring sources may have prevented the counting of all the sources near the cluster centroid.

Robertson and Roach (1990) reported a similar cross-correlation between radio sources in the MRC (408 MHz) survey and clusters in the ACO catalogue. Our power-law fit to their surface densities out to $r/R_{\rm A} = 0{\cdot}33$ (with no correction for background sources) yields an exponent of $-1{\cdot}50$, only slightly lower than the slope of $-1{\cdot}63$ in our Fig. 5, but their surface densities are much lower. This is due to the very different sensitivities of the surveys; assuming a representative spectral index of $\alpha = -0{\cdot}85$, most of the sources in the MRC survey would have $S_{1{\cdot}5} \geq 330$ mJy, which from Fig. 2 constitute only ∼6% of the galaxy identifications in our complete sample. Nevertheless, it is important that the more intense cluster sources (most of which were detected because of a much larger sample of clusters) display a similar radial variation to that of the weaker sources in our samples.

Slee *et al.* (1983) reported an unbiased survey at $2{\cdot}7$ GHz with the Parkes 64 m telescope of a complete sample of 76 Abell clusters with distance classes 3 and 4. Unlike our VLA survey, the clusters were not selected because of the presence of a radio source. The power-law exponent for this sample is $-1{\cdot}43$ but, again, the surface density is much lower than that of our VLA survey and even lower than that of Robertson and Roach. The Parkes $2{\cdot}7$ GHz survey was complete for sources with $S_{2{\cdot}7} \geq 120$ mJy, corresponding to a limit of $S_{1{\cdot}5} \geq 200$ mJy; our Fig. 2 shows that sources with this flux density constitute only ∼12% of the galaxy identifications in our complete sample and, in addition, the $2{\cdot}7$ GHz survey was restricted to clusters of Abell distances 3 and 4.

Unlike our preliminary radial distribution in Paper I, there is no restriction in this analysis on the flux densities of the sources, except for $S_{1{\cdot}5} \geq 2$ mJy. There is little doubt that these radial distributions are almost uncontaminated by background sources because Fig. 5 shows that the surface density of cluster sources is negligible at $r/R_{\rm A} = 0{\cdot}51$. If the number of identified cluster sources in Table 1 out to $r/R_{\rm A} = 0{\cdot}51$ is divided by the number of contributing clusters, an average of $2{\cdot}1$ radio galaxies per cluster is obtained.

4. The Double Sources

The radio doubles comprise a subset of the complete sample of sources with $S_{1{\cdot}5} \geq 2{\cdot}0$ mJy and located within the FWHP circle on the VLA maps. In this subsection, we shall compare the properties of the doubles identified with cluster galaxies (in the manner described in Section 2*b*) with those of the non-cluster doubles. We define a non-cluster double as one with no optical identification, or a double identified with a galaxy that has a measured redshift inconsistent with that of the cluster.

Table 2. Median measured parameters for double radio sources

Sample	Total flux (mJy)	Ratio of fluxes S_a/S_b	Spectral index a	Spectral index b	Ratio of areas a/b	Ratio of SB* a/b
Cluster doubles	165 (27)	1·37 (27)	−1·01 (17)	−0·96 (17)	1·56 (20)	1·14 (20)
Non-cluster doubles	18·6 (48)	1·38 (48)	−0·99 (14)	−0·98 (14)	0·85 (26)	1·38 (26)
All doubles	39·2 (75)	1·37 (75)	−1·00 (31)	−0·97 (31)	1·15 (46)	1·30 (46)

The bracketed number is the number of doubles in each sample.
* Surface brightness (SB) = flux density/angular area.

(4a) Distributions of Component Ratios

Table 2 lists the median values of component ratios for a number of parameters that are peculiar to double radio sources. The median total flux densities of the cluster and non-cluster doubles differ by a factor of 8·9, a value consistent with the latter being about three times more distant than the cluster doubles, assuming that their intrinsic emitted power distributions are similar and a Euclidean universe. Some of the background sources are probably even more distant because, in sampling a larger volume of space, one is more likely to detect powerful FR II radio galaxies. An examination of the apparent magnitudes of the galaxies identified with cluster and non-cluster doubles provides useful information about the relative distances of the two samples. The median values of m_R for the cluster and non-cluster galaxies are 15·8 and 18·3 mag. respectively; the observed m_R were first given atmospheric, galactic and K-corrections applicable to the cluster upon which the galaxy is projected. Therefore, the fact that the non-cluster identifications are, on average, 2·5 mag. fainter places them at distances about three times greater than those of the clusters in a Euclidean cosmology. This agrees with the same factor deduced from the difference in median flux densities between the cluster and non-cluster doubles. In the following discussion, component a of the double has the higher flux density.

The errors in the medians of Table 2 (from the errors reported in the Gaussian fitting program) are 11% in S_a/S_b, 9% in spectral index, 23% in A_a/A_b and 34% in SB_a/SB_b. Therefore, the only significant difference between cluster and non-cluster doubles is in the ratio A_a/A_b. This was confirmed by K–W ranking tests, which showed that the difference between the lobe-area ratios is significant at the 98% confidence level.

It seems reasonable to conclude from these tests that the a component of a cluster double occupies, on average, a larger area than the a component of a background double. We conjecture that this difference is caused by the higher pressure of the hot intra-cluster gas surrounding the lobes of a cluster double, resulting in the more powerful lobe expanding at a higher rate than the weaker lobe.

To investigate the differences between the median ratios in Table 2 in more detail, we have made K–W tests on the distributions of spectral index and surface brightness of the individual components in cluster and background doubles. We have also tested these quantities between the a and b components of each class of double. No significant differences were found in either spectral index or surface brightness.

In the cluster doubles (with measured or implied redshifts), the distributions of component area and surface brightness in the rest frames of the clusters were subjected to K–W tests. The area of the a component was marginally greater than that of the b component with $P = 0{\cdot}09$, but their surface brightness distributions did not differ with $P = 0{\cdot}95$.

Some intrinsic parameters for cluster doubles are listed in Table 3. The values refer to the whole double.

Table 3. Median intrinsic parameters for cluster doubles

Linear distance from centre (kpc)	Log 1·5 GHz power (W/Hz)	Major axis 5% brightness (kpc)	Total source area $(\text{kpc})^2$	Component spacing (kpc)	Absolute red magnitude
340	24·32	190	10048	69·7	−22·36

(4b) Emitted Power/Surface Brightness versus Spectral Index

We investigated in detail the relationship between emitted power and spectral index in the components of cluster doubles. Plots of spectral index versus emitted power for the a and b components considered separately showed that the component spectra become steeper with increasing power; the significance of the regression was higher for the a component. The correlation plot in Fig. 6, in which the a and b components are identified, shows a regression line that has been fitted to the combined sets of points; the regression is significant at $P = 0{\cdot}006$, and shows that the lobe spectrum steepens with increasing lobe power, although the dependence with a slope of $-0{\cdot}23$ is not a strong one.

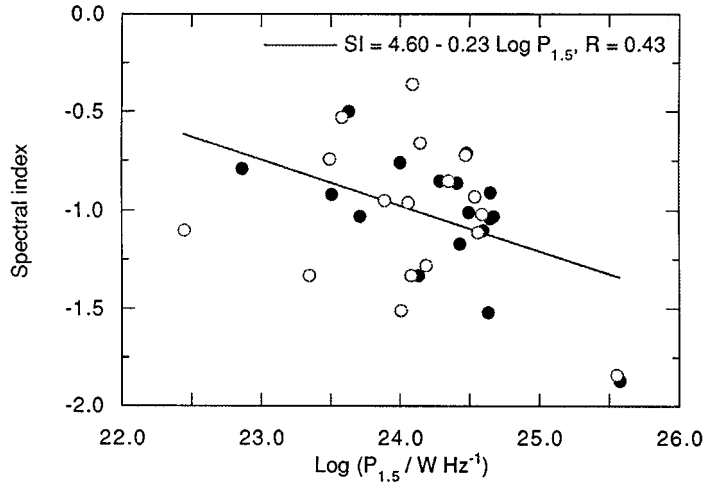

Fig. 6. Correlation between spectral index and emitted power in the lobes of cluster doubles. The stronger (a) lobes are depicted by filled circles and the weaker (b) lobes by open circles. The regression line and its corresponding equation refer to all points. The correlation is significant at $P = 0{\cdot}006$.

The plot of spectral index versus surface brightness in Fig. 7 does not show a very convincing correlation (significance level, $P = 0{\cdot}1$), but does suggest that the component spectra steepen with increasing surface brightness, as they did with emitted power. Figs 6 and 7 show that the lobes of FR I doubles in clusters do not show the spectral-index versus surface-brightness behaviour of double-lobed quasars. Dennett-Thorpe *et al.* (1997) have shown that in the latter, the lobe spectrum flattens with increasing surface brightness, especially in the lobe being energised by a visible radio jet. They attribute this to relativistic beaming and the presence of hot spots in quasar lobes, features that apparently are not present in the lobes of FR I doubles.

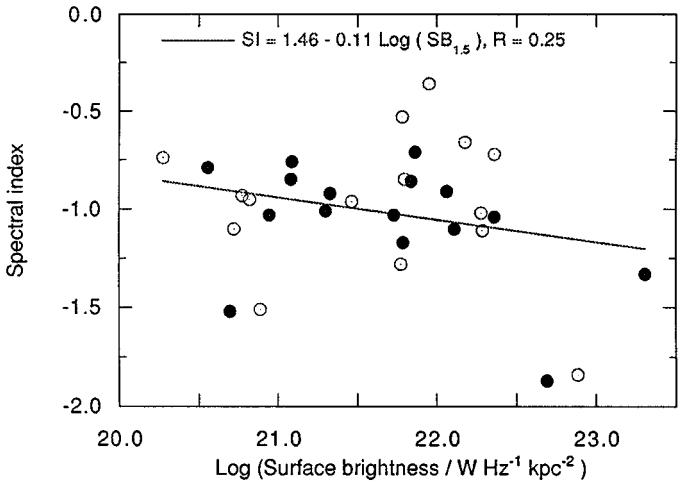

Fig. 7. Correlation between spectral index and surface brightness (in the rest frame) in the lobes of cluster doubles. The stronger (a) lobes are depicted by filled circles and the weaker (b) lobes by open circles. The regression line and its corresponding equation refer to all points. The correlation is significant at $P = 0{\cdot}1$.

In the background doubles (with no redshift data), one can investigate only the relationship between spectral index and surface brightness (defined as the quotient of flux density and angular area). There is no hint of a dependence in these data.

5. Relationships between Intrinsic Parameters in Cluster Radio Galaxies

We tested the correlations between all possible pairs of intrinsic parameters for the two complete cluster samples as defined in Section 2*d*. Such an analysis is not practical for the non-cluster samples because, for them, only three redshifts are available. For these tests, we confine our attention to the radio sources that are identified with galaxies in clusters. Thirty-six of the 41 clusters that were surveyed completely out to $r/R_{\rm A} = 0{\cdot}24$ contained cluster member sources. All 28 of the clusters that had been surveyed completely out to $r/R_{\rm A} = 0{\cdot}51$ contained cluster member sources. In the following analysis we give the results for the sample that is surveyed completely out to $r/R_{\rm A} = 0{\cdot}24$, but we verified the correlations from the second sample surveyed completely out to $r/R_{\rm A} = 0{\cdot}51$. The cluster doubles were included in the analysis.

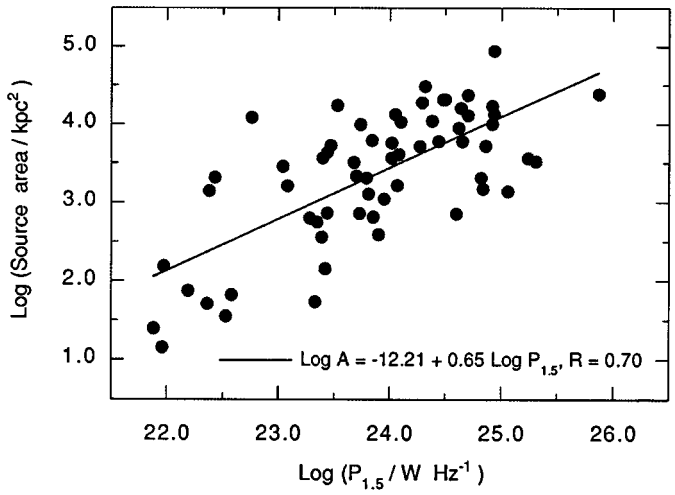

Fig. 8. Correlation between the projected areas of cluster sources and their radio powers from the sample of clusters surveyed completely out to $r/R_{\rm A} = 0{\cdot}23$. The linear regression line and its corresponding equation are shown. The correlation is significant at $P < 0{\cdot}005$.

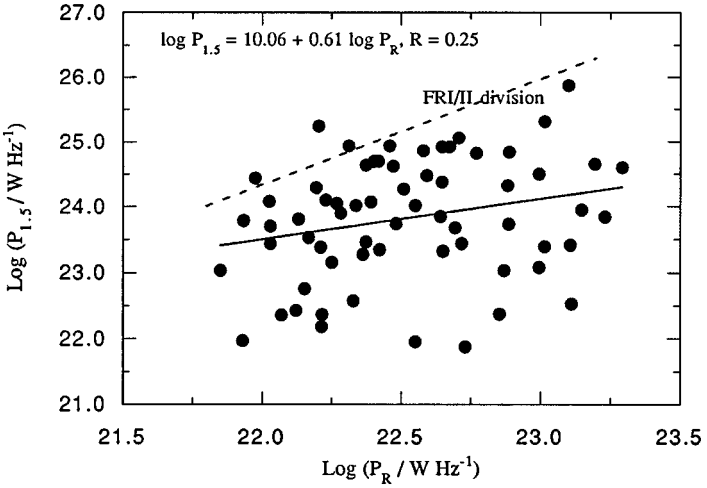

Fig. 9. Correlation between the emitted 1·5 GHz power of cluster sources and the emitted red power of their optical counterparts from the sample of completely surveyed clusters out to $r/R_{\rm A} = 0{\cdot}23$. The filled-in linear regression line and its corresponding equation are shown. The correlation is significant at $P = 0{\cdot}02$. The dashed line shows the division between FR I and FR II radio galaxies, and is explained in Section 5.

Intuitively, the projected area of the source will depend on the radio power, since the latter is likely to partly control the rate of expansion of the lobes into the intra-cluster medium. This correlation is seen in Fig. 8 and is significant at $P < 0{\cdot}005$. It could be argued that such a correlation could be due to the

observational effects of a given brightness sensitivity and the typical brightness gradient in a source. This could result in weaker sources being systematically assigned smaller angular sizes by the Gaussian fitting program (IMFIT). Such an explanation for the strong correlation in Fig. 8 is very unlikely, given that the ratio of peak brightness to map rms for the 16 sources with $S_{1\cdot5} < 20$ mJy has a median value of 45 with 90% in the range 23–127. Therefore the 5% brightness contour (to which the areas in Fig. 8 refer) has a range of 1–6 times the map rms. Fig. 1 in Papers II and III show that a source with peak brightness as low as $0\cdot85\,\mathrm{mJy\,beam^{-1}}$ can easily be traced to the $7\cdot5\%$ brightness contour.

The increase of radio power with R-band optical power shown in Fig. 9 is well known (e.g. Ledlow and Owen 1996). However, it must be qualified by the fact (already introduced in Section $2d$) that there is a luminosity threshold, below which radio galaxies are rarely identified. One is tempted to speculate that, below this threshold, the active nuclei necessary for the formation of radio jets and lobes are not created. For absolute magnitudes brighter than $M_{\mathrm{R}} = -21\cdot0$, the more luminous the galaxy, the more powerful the total radio emission. With a slope of $-0\cdot25$, the dependence of $\log P_{1\cdot5}$ on P_{R} is far from a one-to-one relationship; it accounts for only 6% of the variance in $\log P_{1\cdot5}$, but its significance is high with $P = 0\cdot02$. This dependence will become much clearer when we present the bivariate luminosity functions in Section 7.

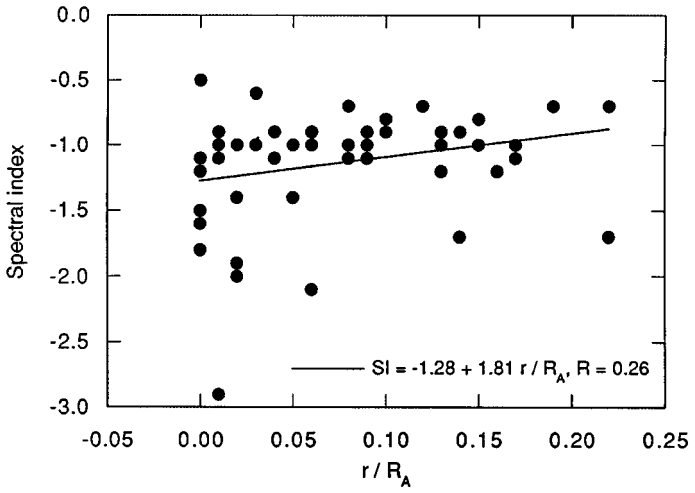

Fig. 10. Correlation between the spectral indices of cluster sources and their angular distances from cluster centres from the sample of clusters surveyed completely out to $r/R_{\mathrm{A}} = 0\cdot23$. The linear regression line and its corresponding equation are shown. The correlation is significant at $P = 0\cdot02$.

Fig. 9 also shows the division between FR I and FR II sources as presented by Ledlow and Owen (1996). Only three of our radio galaxies qualify for inclusion in the FR II classification, and these are associated with galaxies of relatively low R-band power.

The correlation involving spectral index and r/R_{A} (Fig. 10) is significant at $P = 0\cdot03$. It agrees with the claim, already expressed in several publications (e.g.

McHardy 1979; Slee *et al.* 1983), that sources in the relatively dense intra-cluster gas near the cluster centre tend to be confined by the gas pressure, allowing synchrotron and inverse Compton losses to steepen their electron energy spectra over the lifetime of the source.

The correlation between red optical power and $r/R_{\rm A}$ (Fig. 11) is significant at $P < 0{\cdot}005$ and reflects the fact that the higher luminosity cluster galaxies favour the centres of clusters.

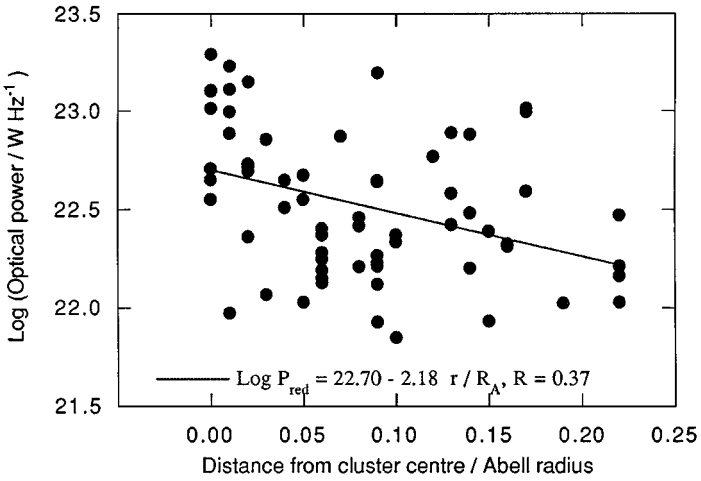

Fig. 11. Correlation between the red optical powers of cluster identifications and their angular distances from the cluster centres from the sample of clusters surveyed completely out to $r/R_{\rm A} = 0{\cdot}23$. The linear regression line and its corresponding equation are shown. The correlation is significant at $P < 0{\cdot}005$.

Since both the radio and optical luminosities were obtained from flux-limited surveys, regressions involving one or both of these quantities may be affected by Malmquist bias. Verter (1993) gave a method of correcting regression analysis for this effect by weighting the individual luminosities by the maximum volume $V_{\rm m}$ sampled at each observation. The method was applied to the three regressions involving luminosities. The main effect was to change the slope of the regression line, but to leave the correlation coefficient relatively unchanged; in one case, radio power versus red optical power, the correlation coefficient was increased from $0{\cdot}25$ to $0{\cdot}31$.

6. Polarisation Measurements

Our polarisation measurements were briefly described in Section 3 of Paper II, where we showed the observed E-vectors superimposed on the radio maps and gave the range of polarisation fraction over each map in Table 2. In this paper we make a more thorough analysis and examine the amount of depolarisation introduced by differential Faraday rotation and tangled magnetic fields in cluster radio sources. For the resolved doubles, we derived the polarisation parameters of their components separately. Thus the measurements consist of data for slightly-resolved sources and the components of resolved doubles. We group these data together for the following analysis.

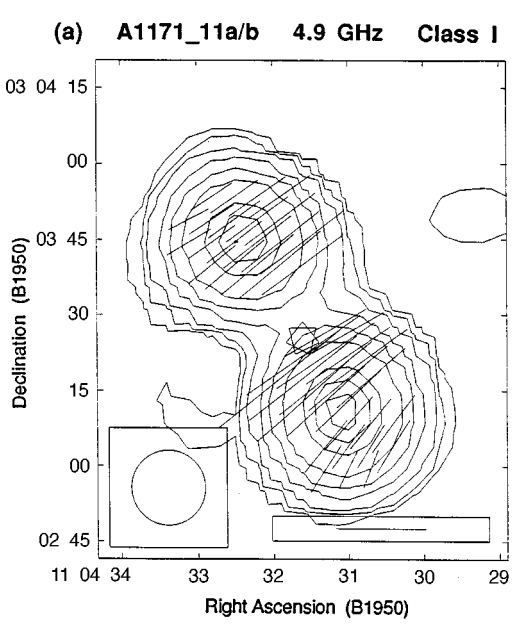

Calibration vector = 10%; peak brightness = 18.1 mJy beam^{-1}; lowest contour = 0.5%

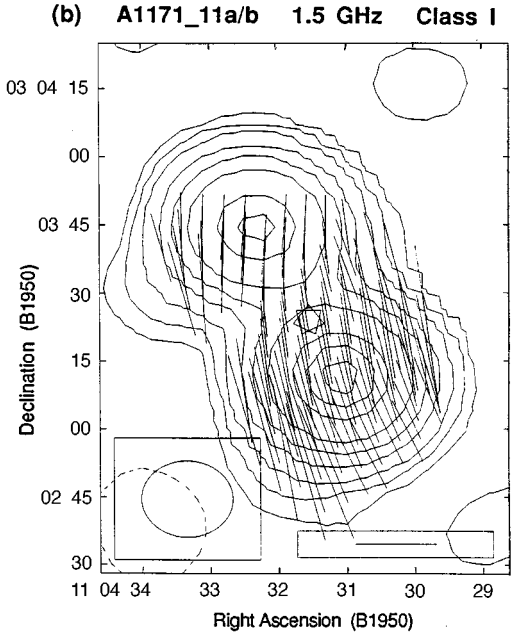

Calibration vector = 10%; peak brightness = 66.8 mJy beam^{-1}; lowest contour = 0.5%

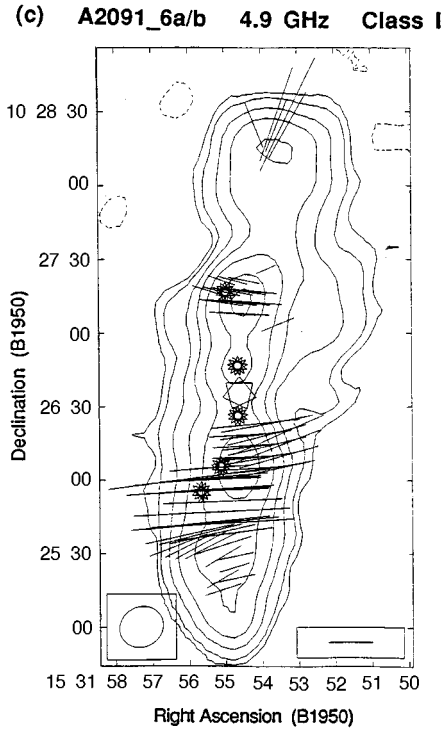

Calibration vector = 10%; peak brightness = 11.4 mJy beam^{-1}; lowest contour = 1.0%

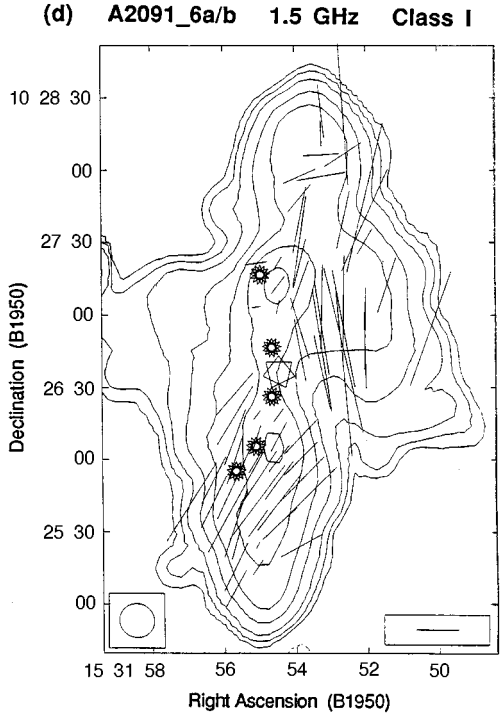

Calibration vector = 10%; peak brightness = 32.7 mJv beam^{-1}: lowest contour = 0.5%

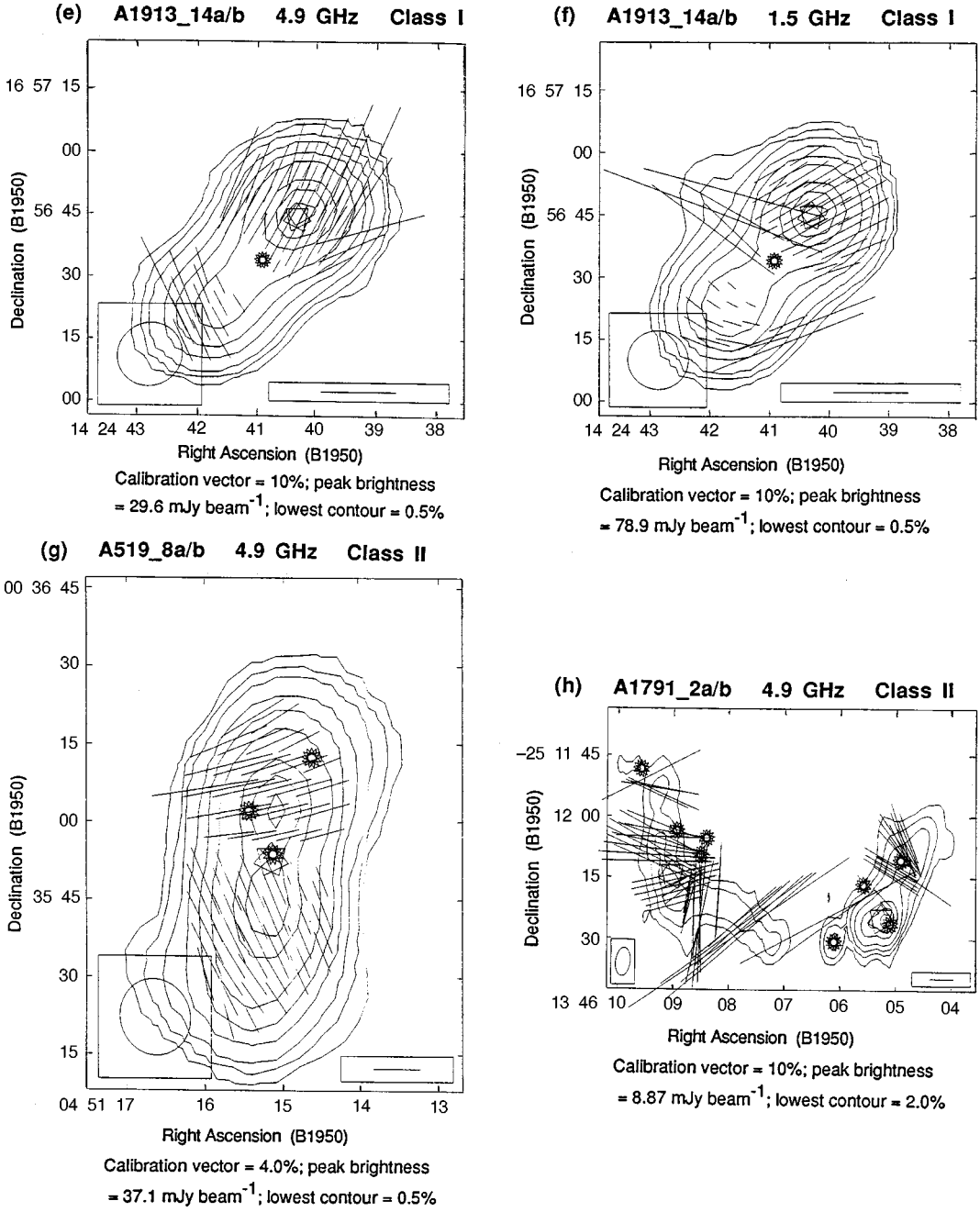

Fig. 12. Contour maps of double sources with superposed electric vectors. The 1·5 GHz maps are from the C-array; while the 4·9 GHz maps are from the D-array, except that A1791__2a/b is from the C-array. The restoring beam to FWHP is in the lower left corner. The rms level in each map is listed in Table 1 of Paper III. The calibration vector in the box in the lower right corner represents a polarised fraction of 10%, except that for A519__8a/b it represents 4%. Radio positions are represented by 7-pointed stars, and positions of galaxies by 13-pointed stars.

In Paper II we arbitrarily assigned a lower limit to the measurable polarisation of 5% of total intensity. For this paper we estimated the instrumental polarisation by comparing the measured polarisation fractions for 25 calibrator sources used in our VLA observations with the polarisation fractions reported for the same sources by Perley (1982). We found that the instrumental polarisation was always <2% and usually <1% of total intensity. We also investigated how the rms noise levels on the polarisation maps affects the limit of measurable polarisation. If the 5-sigma noise level fell below 2% of the source's peak brightness on the Stokes-I image (as it did for most source components), we adopted a limit of 2% for the measurable polarisation. For the remaining few source components, we adopted the higher limit of 5 times the rms noise.

The minimum-energy magnetic field $B_{\rm me}$ within each source component (corresponding approximately to energy equipartition between field and relativistic particles) was computed from equation (2) in Section 3·1 of Miley (1980). This could be done only for the cluster sources with measured or implied redshifts. We used $k = 1$, $\eta = 1$ and $\sin\varphi = 1$, these being, respectively, the ratio of energy in protons to that in electrons, the filling factor of the relativistic plasma with respect to the entire source volume, and the angle between the field and line-of-sight. The spectral index, which has an important influence on $B_{\rm me}$, is the measured value given in Paper II. Most of the variable factors in the computation affect the result only as the 2/7 power, and departures from the assumed values usually act to increase the field strength. As an example, reducing the filling factor from 1·0 to 0·1 increases $B_{\rm me}$ by only 16%. Another uncertainty is the assumption of equipartition itself. However, comparing the thermal pressure of the X-ray emitting gas surrounding 22 low-luminosity radio galaxies to their internal non-thermal pressure (based on $B_{\rm me}$), Morganti *et al.* (1988) found that external and internal pressures are usually in reasonable equilibrium. Only for tailed radio sources is a noticeable deviation from equipartition apparently necessary to equalise the internal and external pressures (Feretti *et al.* 1992).

(6a) Polarisation Classes and Polarised Structure

Since the polarisation maps at 1·5 and 4·9 GHz were obtained with scaled arrays (to ensure approximately equal angular resolution at both frequencies), the measured reduction in polarisation fraction at 1·5 GHz compared with that at 4·9 GHz is a true measure of the so-called depolarisation ratio D, where $D_{1\cdot5 \text{ to } 4\cdot9} = \mathrm{Pol}_{1\cdot5/\mathrm{Pol}\,4\cdot9}$, Pol_ν being the polarised fraction at frequency ν. The sources or resolved components of doubles may be allocated to three classes:

Class I, where the polarised fraction is measurable at both 1·5 and 4·9 GHz.

Class II, where the polarised fraction is measurable at 4·9 GHz, but not at 1·5 GHz.

Class III, where the polarised fraction is measurable at neither frequency, i.e. $\mathrm{Pol}_\nu < 2\%$.

A representative sample of contour maps with superposed electric vectors is presented in Fig. 12 for some Class I and Class II sources. Figs 12*a* and 12*b* refer to the Class I double, A1171_11a/b, in which the components are poorly resolved with lobe/beam diameter of ∼0·3, so that the observed polarised fractions of ∼12% at 4·9 GHz and 10% at 1·5 GHz are effectively averages over the lobes. The electric vectors at 4·9 GHz are near-perpendicular to the axis of the double

and a comparison of the average vector directions at 4·9 and 1·5 GHz yields a RM of $\sim+29$ rad m^{-2} in both lobes.

Figs 12*c* and 12*d* relate to the well-resolved Class I double, A2091__6a/b, with lobe/beam diameter ∼3. Here, we see the patchy nature of the polarised emission, which when averaged over the lobes, gives polarised fractions of ∼16% at 4·9 GHz and ∼14% at 1·5 GHz. Again, it is clear that the electric vectors at 4·9 GHz are near-perpendicular to the double's axis. A comparison of the directions of the vectors at 4·9 and 1·5 GHz yields RM of -16 and $+14$ rad m^{-2} for the northern and southern lobes respectively. The beam diameter at the source is 35 kpc, so it is safe to assume that the scale size of tangled fields must be $\ll$35 kpc if the polarised fraction at 4·9 GHz is only 21% of the theoretical maximum.

Figs 12*e* and 12*f*, for the poorly resolved Class I double, A1913__14a/b, with a lobe/beam diameter of ∼0·3, show an unusual rotation of the electric vector of 54° between the lobes. The deduced RM are -16 and $+14$ rad m^{-2} for the NW and SE lobes respectively. If the difference in PA at 4·9 GHz were due solely to Faraday rotation, the implied difference in RM is 250 rad m^{-2}, which clearly disagrees with the measured difference of 30 rad m^{-2}. This indicates, rather, that the average field directions in the lobes differ by 54°.

Fig. 12*g* is a polarisation map of the Class II double, A519__8a/b, with a lobe/beam diameter of ∼0·5. The averge 4·9 GHz polarised fraction is 5% for both lobes, but the vector is rotated by ∼90° between them. If this rotation is due to Faraday rotation, the implied difference in RM is ∼400 rad m^{-2}, but it seems more likely that the difference is caused by a flip of 90° in the direction of the average field.

Finally, Fig. 12*h* shows the 4·9 GHz polarised structure in the very well resolved Cluster WAT, A17912a/b (observed in the scaled B/C configurations). This is a Class II source with each lobe having an angular size of several beamwidths. The patchy nature of the polarised emission is very clear with the polarised fraction averaging 30–42% and, generally, with the electric vector near-perpendicular to the axes of the lobes. The equivalent circular beam at the source has a diameter of 10 kpc, and the high fractional polarisation of up to 56% of the theoretical limit means that the scale of the tangled fields is almost resolved.

Table 4 gives some median values for the parameters in the three classes and also shows the results of K–W ranking tests on the distributions of each parameter. The parameters intrinsic to the source can be given only for the fraction identified as cluster members and therefore with measured or implied redshifts. We have excluded the polarised quasar A154__5iii from this statistical study and the cluster WAT, A1791__2a/b, which was observed with three-times better angular resolution than the remainder of the polarised sources (see the last paragraph).

(6b) Depolarisation in Radio Sources

Two basic mechanisms contribute to a reduction in the observed polarisation from the theoretical value of ∼75% at the emission location in the source. These mechanisms are:

(1) Changes in field directions across and into the source (tangled fields).
(2) Changes in Faraday rotation of the electric vector across and into the source and/or in any ionised gas surrounding the source, including the intra-cluster gas.

Table 4. Parameter distributions of polarisation classes

Parameter	Units	Class I		Class II		Class III		Significance
		No. sources*	Median	No. sources*	Median	No. sources*	Median	level†
4·9 GHz								
polarisation#	%	23	8·1	20	8·0	27	≤2·0	0·99
1·5 GHz								
polarisation#	%	25	5·8	20	≤2·0	27	≤2·0	
Depolarisation ratio		23	0·82	20	≤0·25			
Rotation measure (|RM|)	rad m^{-2}	23	22·1					
Spectral index		25	−1·01	20	−0·96	27	−1·12	0·01
Lobe diam./Beam diam.		25	0·38	20	0·63	27	0·43	0·10
Lobe area	$(\mathrm{kpc})^2$	13	714	16	255	19	83·7	<0·005
Lobe diameter	kpc	13	30·1	16	18·0	19	10·3	<0·005
Log surface brightness	$\mathrm{W/Hz/(kpc)^2}$	13	20·92	16	21·61	19	21·87	<0·005
Magnetic field B_{me}	μG	13	7·6	16	11·7	19	24·9	<0·005
Abs. red magnitude	mag.	13	−21·96	16	−22·36	19	−22·91	<0·005
Dist. from cluster centre	r/R_{A}	13	0·10	16	0·10	19	0·01	<0·005

* In resolved doubles, the components are treated separately.
† Kruskal–Wallis ranking test probability of the distributions being from the same parent population.
# Denotes the average polarisation over the source.

Table 5. Polarisation correlations

Regression	Number of pairs	Correlation coefficient	Chance probability	Regression equation	Units
4·9 GHz polsn vs 1·5 GHz polsn	23	0·68	<0·005	%4·9 = 3·44+0·71 (%1·5)	%, %
4·9 GHz polsn vs Lobe area/Beam area (LA/BA)	44	0·46	<0·005	%4·9 = 6·95+1·77 (LA/BA)	%
4·9 GHz polsn vs Surface brightness (SB)	27	0·36	0·03	%4·9 = 73·45–3·02 Log(SB)	%, $\mathrm{W/Hz/kpc^2}$
4·9 GHz polsn vs Source diameter (SD)	27	0·44	0·01	%4·9 = 5·73+0·135 (SD)	%, kpc
Minimum field (B_{me}) vs Abs. mag. (M_{R})	27	0·59	<0·005	$B_{\mathrm{me}} = -340{\cdot}3 - 16{\cdot}05\ M_{\mathrm{R}}$	μG, mag.

Clearly, the magnitude of the depolarisation depends in both mechanisms upon the angular resolution of the telescope and the scale sizes of both field and thermal electron density variations—the more averaging over the radio beam, the greater the reduction in the observed polarised fraction. In our VLA experiment, the effects of tangled fields are very similar at $1{\cdot}5$ and $4{\cdot}9$ GHz, since we were using almost identical resolution at the two frequencies. The magnitude of Faraday depolarisation will depend both on the angular resolution and the radio frequency, the latter dependence being due to the fact that the rotation measure (RM) is proportional to λ^2. Again, the averaging due to the antenna beam will be similar at the two frequencies, a characteristic that allows us to unambiguously measure the depolarisation due to differential Faraday rotation by comparing the ratio of polarisation fractions at $1{\cdot}5$ and $4{\cdot}9$ GHz.

The basic theory of depolarisation is presented by Burn (1966) and Cioffi and Jones (1980), who showed that similar quantitative results apply to slab, spherical and cylindrical models of the depolarising region. The observed Faraday rotation and depolarisation may occur in the source itself or during propagation to the observer, the latter including the intra-cluster, galactic and local ionospheric media. During our experiment, the rotation measure RM in the ionosphere was negligible and will be ignored in the following discussion. The galactic RM can be significant, depending rather critically on galactic latitude and, to a lesser extent, on galactic longitude. However, from Table 1A in Kim *et al.* (1991) we estimate the galactic contribution to have a median of $|6|$ rad m^{-2} from their 81 sources with $40{\cdot}0^\circ \leq |b| \leq 70{\cdot}0^\circ$, which is the range of galactic latitude for most of our sources.

In the following subsection we shall be making use of the concepts of 'depolarisation ratio' (D) and 'Faraday depth' (F), which we define as

$$D_{1\cdot5-4\cdot9} = \mathrm{Pol}_{1\cdot5}/\mathrm{Pol}_{4\cdot9}\,, \tag{1}$$

where Pol_ν is the polarised fraction at frequency ν, and

$$F(\lambda) = 1600\ n_\mathrm{e} B_\mathrm{p} \lambda^2 L\,, \tag{2}$$

where n_e is the thermal electron density cm^{-3}, B_p is the field parallel to the line-of-sight in μG, λ is the wavelength in m, and L is the source depth in kpc. We shall also need the rotation measure defined as

$$\mathrm{RM} = 8{\cdot}1 \times 10^2\ n_\mathrm{e} B_\mathrm{p} L\,, \tag{3}$$

where the units are rad m^{-2}. The Faraday rotation angle χ (in degrees) can be found from

$$\chi = 57{\cdot}3(\mathrm{RM})\lambda^2\,. \tag{4}$$

Equations (2) and (3) assume that the magnetic field direction throughout the source is constant in both value and direction and that, likewise, the thermal electron density is constant. If these values vary throughout the source, then equation (2) must be expressed as an integral over all values of $n_\mathrm{e} B_\mathrm{p}$ throughout the source. Wavelength-dependent depolarisation depends upon $f(\phi)$, the variation from point to point in the source of the Faraday depth,

$$\phi = \int n_{\rm e} B_{\rm p} \, {\rm d}l \, , \tag{5}$$

where $B_{\rm p}$ is the component of the field parallel to the line-of-sight and the integration is carried out along the line-of-sight from the volume element to the observer. Burn (1966) showed that one cannot deduce the distribution function $f(\phi)$ directly from the observations but that, by assuming a source model and a Gaussian distribution for $f(\phi)$, one can express the dispersion in $f(\phi)$ in terms of the observed depolarisation ratio D between $4{\cdot}9$ and $1{\cdot}5$ GHz. For the thick-slab model, the Faraday dispersion is

$$\Delta = 21{\cdot}92(-\ln D)^{\frac{1}{2}} \, , \tag{6}$$

where the units are $\rm cm^{-3}\,\mu G\,pc$.

(6c) Depolarisation in Cluster Sources

Even in the complete absence of thermal electrons in the source, the existence of a highly tangled field structure would ensure a high degree of wavelength-independent depolarisation, provided the scale size of field reversals is much smaller than the linear size of the antenna beam at the source. Burn (1966) showed that the reduction factor is approximately the energy in the uniform field divided by the energy in the total field. Even in those of our Class I sources with depolarisation ratios $D \sim 1$, the average polarisation fraction never exceeds $\sim$15% in the scaled C/D arrays (i.e. 20% of the theoretical maximum). Therefore, one is persuaded that the energy in a unform field can be no more than a fifth of the total magnetic energy. The wavelength-dependent depolarisation (defined by D) depends upon the Faraday dispersion Δ and can only contribute a small amount of the total depolarisation in Class I sources (median $D = 0{\cdot}82$); the median Faraday dispersion from (6) is $\Delta = 9{\cdot}8\ {\rm cm^{-3}}\ \mu$G cm.

Faraday dispersion contributes more to the depolarisation of Class II sources. Their median depolarisation ratio of $D \leq 0{\cdot}25$ (Table 4) gives $\Delta \geq 25{\cdot}8\ {\rm cm^{-3}}$ μG cm. There is no reason to believe that most of the depolarisation at $4{\cdot}9$ GHz is not due to the tangled nature of the magnetic fields in the source—it is the much stronger depolarisation at $1{\cdot}5$ GHz (compared with Class I) that is due to the higher Faraday dispersion.

In Class III sources Faraday dispersion is clearly much higher, although it is not possible to estimate it without a measurement of the depolarisation ratio. It is high enough, however, to reduce the maximum polarisation seen in Class I and II sources at $4{\cdot}9$ GHz from $\sim$15% to $\leq$2% in Class III sources.

It is clear from the last column in Table 4 that the classes differ significantly in the intrinsic parameters of linear source size, surface brightness and minimum-energy magnetic field strength, although the three parameters are not entirely independent; this is because both surface brightness and computed $B_{\rm me}$ involve the linear dimensions, as well as the emitted power, in one form or another. It is possible to state that, while the source volume decreases systematically from Class I to Class III, the surface brightness and minimum-energy field increase systematically. Although the distributions of (source diameter)/(beam diameter) for the three classes differ only marginally, we show in Section 6*d* that the angular resolution has an important influence on depolarisation.

Table 4 also shows that the cluster sources in Class III are much closer to their cluster centres than those in Classes I and II, and are associated with the intrinsically brightest galaxies.

(6d) Correlations between Parameters

Table 5 presents the results of linear regression analysis between pairs of parameters involving all the sources in Table 4. All but one of these regressions involves the fractional polarisation at 4·9 GHz and almost every other available parameter. Regressions involving intrinsic parameters are necessarily confined to cluster sources, which are identified with galaxies that have the measured or assumed redshift of the clusters.

The most significant correlation is between the 4·9- and 1·5-GHz polarised fractions in Class I sources, which accounts for 48% (square of the correlation coefficient) of the variance; this is basically because the emitted polarisation fraction is independent of frequency (Pacholczyk 1970). Another important correlation is that between 4·9-GHz polarised fraction and (lobe area)/(beam area); this shows that the polarised fraction increases with the degree of angular resolution, although the correlation accounts for only 23% of the variance. This relationship measures the beam depolarisation in our data, which we first introduced in Section 6*c*. The depolarisation due to lack of angular resolution is nowhere better illustrated than in the cluster source A1791_2a/b, which was observed with the scaled B/C arrays (compared with the scaled C/D arrays for the sources in Tables 4 and 5). The resulting three-fold increase in angular resolution resulted in our measuring average polarised fractions at 4·9 GHz of 30% and 42% for the a and b components respectively.

Other noteworthy correlations are between polarised fraction and surface brightness and between polarised fraction and minimum field strength, although they account for only 15% and 9% of the variance respectively; note, however, that the dependent variables are linked through their dependence on radio power and linear dimensions. Perhaps an unexpected result is the significant correlation between minimum energy field and absolute magnitude, although this could be explained by the fact that both variables are related to the emitted radio power.

(6e) Location of the Depolarising Region and Faraday Rotation

We have already shown in Section 6*c* that most of the depolarisation can occur in the source itself due to small scale field reversals. Here we wish to decide whether the smaller frequency-dependent part of the deplolarisation in Class I and II sources is internal or external and where the observed Faraday rotation occurs. To help answer these questions, we have adopted the method of Garrington and Conway (1991) as applied to the lobes of quasars and FR II radio galaxies. These authors show that if Faraday depolarisation and rotation occur in the same ionised medium, there should be a strong correlation between Faraday RM and Faraday dispersion Δ as given by equation (6) in Section 6*b*. Fig. 13 shows a scatter plot of these quantities for the 23 lobes in polarisation Class I. There is no significant correlation.

In order to eliminate complications due to the poorly known local Galactic contribution to RM, one plots the differences in RM, $|\Phi_a - \Phi_b|$, against the differences in Faraday dispersion $|\Delta_a - \Delta_b|$, where a and b refer to the lobes

of a double source. This procedure is based on the reasonable assumption that the Galactic RM will not change significantly over the angular separation of the lobes, yielding a result that is independent of the Galactic RM.

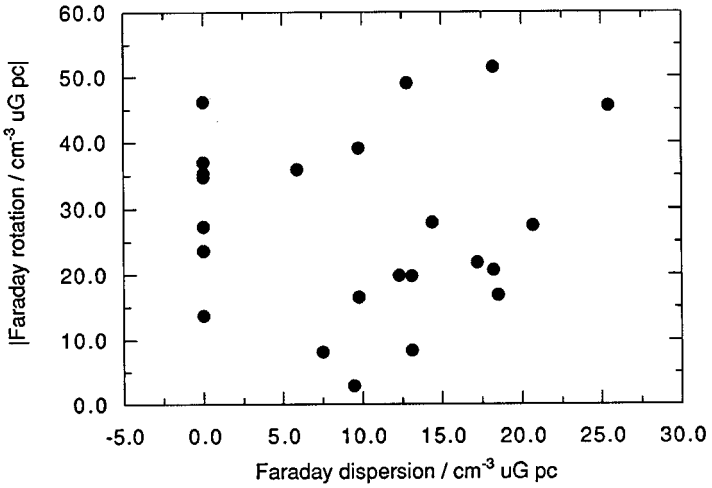

Fig. 13. Faraday rotation measure RM plotted against Faraday dispersion Δ for the lobes of doubles in polarisation Class I. The correlation is not significant.

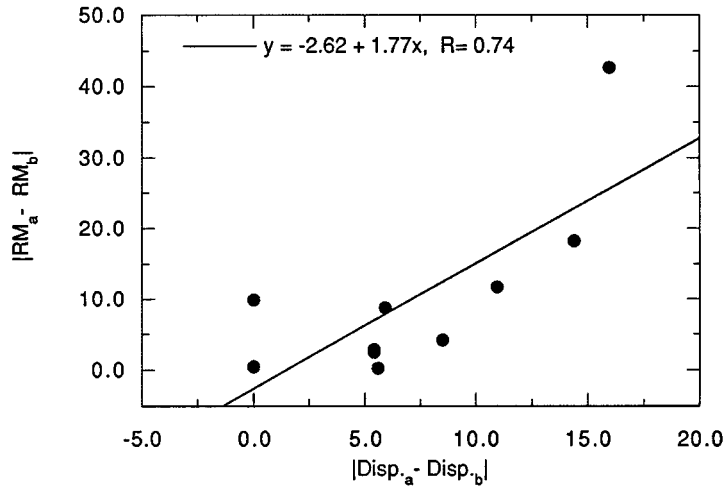

Fig. 14. Difference in Faraday rotation measure plotted against difference in Faraday dispersion for the pairs of lobes of doubles in polarisation Class I. Units on both axes are cm^{-3} μG pc. The fitted regression line and its equation are shown. The correlation is significant at $P = 0{\cdot}006$.

Fig. 14 shows the result of applying this method to the 10 doubles in Class I with polarisation detections in both lobes; we find a correlation coefficient of $0{\cdot}74$, which is significant at $P = 0{\cdot}006$. This contrasts with the negative result obtained by Garrington and Conway (1991) for quasars and FR II radio galaxies,

and by Morganti *et al.* (1997) for a large sample of field FR I radio galaxies. Our conclusion is that the Faraday rotation and Faraday depolarisation take place in the same ionised gas. Since small-scale depolarising structure is known to exist in the source plasma (from the wavelength-independent depolarisation seen in Class I), it is likely that the Faraday depolarisation also occurs in the entrained thermal gas in the source. However, Garrington and Conway (1991) and Morganti *et al.* (1997) claim that *both* the depolarisation and rotation are likely to occur in an ionised halo surrounding the source, despite the fact that they found no correlation between Faraday rotation and dispersion.

If the Faraday rotation and depolarisation occurs in the intra-cluster gas, one may expect a correlation between the electron density and/or temperature as deduced from L_x and kT. Only five of the lobes in Class I with RM measurements are in clusters having published X-ray measurements. Therefore, we have used the more numerous RM results of Kim *et al.* (1991) for sources with projected distances from cluster centroids $r/R_{\rm A} \leq 0{\cdot}33$. Twenty-seven of these sources are associated with clusters having ROSAT measurements from Ebeling *et al.* (1996). We found *no significant* correlation between RM and $L_{\rm x}$ or between RM and kT. We therefore conclude that the observed Faraday rotation and depolarisation are unlikely to originate in the intra-cluster gas itself, despite the fact that Kim *et al.* (1991) showed conclusively that sources with $r/R_{\rm A} \leq 0{\cdot}33$ possess a median RM that is 3–4 times higher than that of sources with $r/R_{\rm A} > 0{\cdot}33$. One way of reconciling these apparently conflicting data is to postulate that the thermal gas entrained in the source is *indirectly* increased by its proximity to the densest region of the intra-cluster gas, possibly through cooling flows.

(6f) Thermal Plasma associated with Class I and II Sources

In this subsection we are concerned with interpreting the depolarisation measurements on the sources identified as cluster members, which provide the intrinsic parameters for Class I and II sources in Table 4. We have already shown in Section 6*c* that much of the depolarisation could be due to the existence of tangled fields, irrespective of the presence of entrained thermal gas. For these calculations we assume that the Faraday depolarisation occurs in the source itself, as explained in Section 6*e*.

We assumed in Section 6*b* that there is a Gaussian distribution of Faraday depths with rms dispersion Δ, which is given by

$$\Delta = \langle n_{\rm e}^2 B_{\rm p}^2 \rangle^{\frac{1}{2}} (Ld)^{\frac{1}{2}} \,, \tag{7}$$

where $n_{\rm e}$ ($\rm cm^{-3}$) and $B_{\rm p}$ (μG) are the electron densities and field components parallel to the line-of-sight, L (kpc) is the source thickness and d (kpc) is the rms scale size of the depolarising elements. There is considerable evidence from Section 6*a* (reinforced by our analysis of the polarised structure in 14 well-resolved Class I and II sources in Section 6*g*), that d is <10 kpc, so we adopt a value of $d = 5$ kpc.

Substituting in (7) for the median values of B and L for Class I sources from Table 4 and $\Delta = 9{\cdot}8\ \rm cm^{-3}\ \mu G$ pc, we obtain $\langle {n_{\rm e}}^2 {B_{\rm p}}^2 \rangle^{1/2} = 0{\cdot}80$. Now if we assume that the rms value equals the average, then $\langle n_{\rm e} \rangle = 1{\cdot}1{\times}10^{-4}\,\rm cm^{-3}$. Substituting the medians in Table 4 for the Class II sources and with $\Delta \geq 25{\cdot}8\,\rm cm^{-3}$ μG pc, we obtain $n_{\rm e} \geq 2{\cdot}3{\times}10^{-4}\,\rm cm^{-3}$.

The entrained thermal electron density in polarisation Class III must be considerably higher and probably approaches the the typical intra-cluster gas density of $3\times10^{-3} \leq n_e \leq 10^{-2}\,\mathrm{cm}^{-3}$ obtained by Pislar *et al.* (1997) within the core region of Abell 85. We note from Table 4 that the median projected source-cluster centre spacing is only 20 kpc for Class III sources, contrasting with the 200 kpc spacing for Classes I and II.

The presence of a cooling flow may lead to the increase in the entrained thermal gas seen in Class II and especially Class III sources. Fabian (1994) suggested that from the available X-ray evidence, some 70–80% of the clusters possess cooling flows, which generate a pronounced enhancement in electron density within the central 100-kpc radius. Of the verified cluster sources, 38% of Class II sources and 58% of Class III sources are situated within this radius. Our polarisation data summarised in Table 4 include sources from five clusters with well-observed cooling flows: A496__4, A1689__15a/b, A2029__2a/b, A2052__1, and A4038__11. The polarisation fractions of these sources are $\leq 2\cdot0\%$ at both $4\cdot9$ and $1\cdot5$ GHz, i.e. they are Class III sources. The RM of A2052__1 has been mapped with high angular resolution by Ge and Owen (1994), who found that its RM varied between +500 and −500 rad m^{-2} over the source, and they measured polarised fractions of up to 40% at $3\cdot6$ cm wavelength. Thus we conclude that our poorly resolved image of this source at $4\cdot9$ GHz is depolarised partly because of differential Faraday rotation and partly because of tangled fields.

(6g) Directions of Magnetic Fields

The lack of sufficient angular resolution, combined with only lower limits to RM in our polarisation classes II and III, do not permit us to derive unambiguous field directions for most of the components in Table 4; we shall be able to do so for only the better resolved sources in Class I, where the depolarisation is mainly caused by tangled fields and the measured median RM of $22\cdot1$ rad m^{-2} ensures that only small corrections to the observed position angles are necessary at $4\cdot9$ GHz.

We have focussed our attention on the 21 lobes of Class I doubles with measured RM. The lobes of doubles (rather than the whole source) are treated separately in the following discussion, because in two doubles we can detect polarisation in only one of their lobes, and in three doubles the electric vector changes by angles between 50° and 69° from one lobe to the other. In all cases we averaged the position angle of the $4\cdot9$ GHz electric vector over the radio lobe (average standard error ∼3°) and we have corrected for Faraday rotation (average correction $\sim|5|^\circ$).

In Fig. 15 we show the distribution of the differences between the corrected E-vector position angles at $4\cdot9$ GHz for 21 lobes in Class I doubles and the main axes of their respective doubles (given in Table 3 of Paper II). A test for a fit with a uniform distribution gives $\chi^2 = 21\cdot4$ with 8 degrees of freedom, so that the observed distribution has a probability $P < 0\cdot01$ of having been drawn from the parent population of uniform distributions.

It is apparent from Fig. 15 that a small fraction of the lobes of Class I doubles have E-vectors that make small or intermediate angles with the double's axis—an example can be seen in Fig. 12*e* for A1913__14a. In the two extreme cases with angles of ∼15°, the other lobe of each pair conforms with the majority. Neither

of the deviant lobes possesses an extreme RM, although a sign change takes place between the lobes in these doubles.

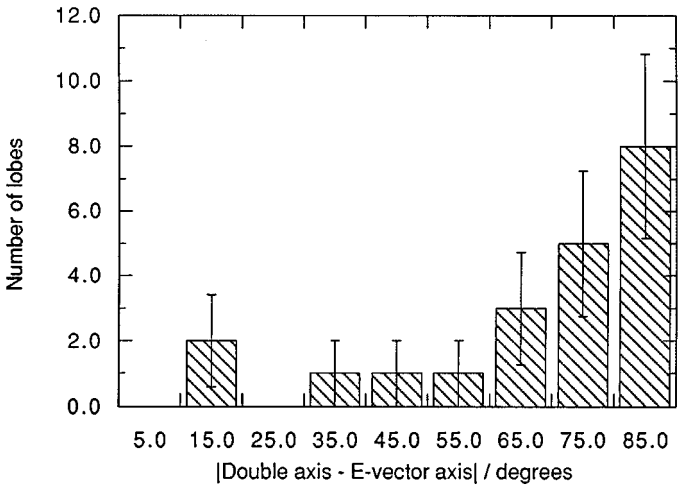

Fig. 15. Distributions of the differences between the position angles of E-vectors and the axes joining the lobe centroids in cluster doubles of polarisation Class I. The Poisson sampling errors of $\pm\sqrt{N}$ are shown.

A plot similar to Fig. 15 was constructed for the lobes of Class II doubles, this time without the benefit of RM correction. The resulting distribution of angles, |double axis $-$ E-vector|, has a probability of $P = 0{\cdot}35$ of having been drawn from a population of uniform distributions. This result is another indicator of the higher |RM| in Class II sources—an example of such a double can be seen in Fig 12g.

In summary, Fig. 15 shows that the magnetic field (perpendicular to the E-vector in optically thin sources) favours a direction parallel to the axis of a double and, presumably, the unresolved jets. This conclusion agrees with the result obtained by Morganti *et al.* (1997) for a large sample of FR I field doubles.

(6h) Scale Size of Polarised Structures

The well-resolved doubles in Fig. 12 show that polarisation is often very patchy. In extreme cases, one lobe of a double may be polarised (though often in only one area of the lobe), while the other may show no detectable polarisation (i.e. $<$2% in our analysis). We have already shown in Section 6c that the Class I doubles, in which polarisation can be detected at both $1{\cdot}5$ and $4{\cdot}9$ GHz in the same areas of the lobes, are predominantly depolarised in these common areas because of tangled fields across the radio beam; this suggests that the scale of field reversals, both across the beam and into the source (all sources are optically thin), is considerably smaller than the linear size subtended at the source by the beam. In polarisation Classes II and III, in which Faraday depolarisation is significant, the scale of the thermal plasma is also acting to determine the scale of the polarised emission. We have shown in Sections 6e and 6f that the thermal gas is probably entrained with the radio-emitting plasma, so that the scale size is common to the emitting and depolarising processes.

We have examined the 4·9-GHz maps of 14 well-resolved Class I and II sources with redshifts and we have measured the areas (pixels) of the polarised regions that have approximately the same polarisation fractions and/or position angles. Depending on the degree of resolution of the source or lobe, one could identify up to eight such polarised areas (e.g. A1791_2a/b in Fig. 12*h*). The pixel areas were converted to the angular diameters of the equivalent circular areas and transformed to linear diameters via the redshifts.

A histogram of the distribution of the diameters of polarised regions is shown in Fig. 16, which has a broad peak in the 5 to 20 kpc range of diameters. The median linear diameter is 13·9 kpc, but it is clear from a significant regression of polarised-region diameter on linear beam diameter (not plotted) with a correlation coefficient 0·67 for 48 pairs, that the polarisation structure is not being resolved in most sources. At the highest resolution (∼5 arcsec for A3528_1a/b and A1791_2a/b) depicted by the stippled area in Fig. 16, the patch diameters are 3–10 kpc, and the polarisation fraction is up to 56% of theoretical maximum. This is an important statistic in considering the scale of turbulence in cluster radio galaxies. From this evidence, we have used an rms scale diameter of 5 kpc in Section 6*f* to derive electron density in the entrained thermal gas.

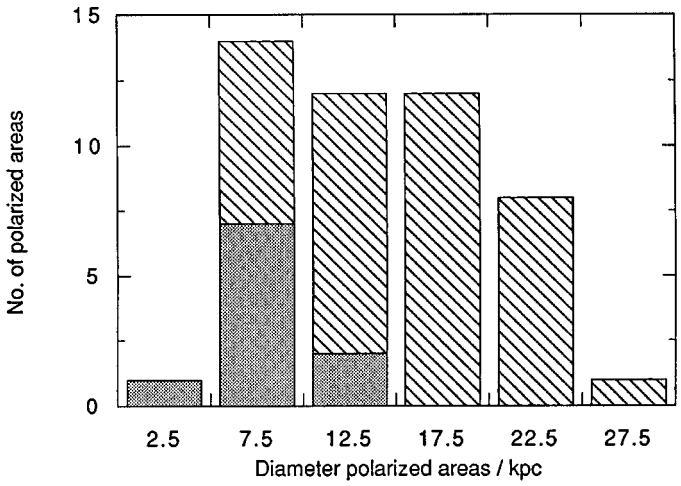

Fig. 16. Distribution of 4·9 GHz diameters of discrete polarised areas in the lobes of well-resolved doubles in polarisation Classes I and II. The stippled area represents the counts for doubles observed with ∼4 arcsec resolution and the cross-hatched area for doubles observed with ∼14 arcsec resolution.

7. Radio Luminosity Functions

We have chosen to follow the methods used by Ledlow and Owen (1996) in their comprehensive discussion of the radio luminosity functions (RLF) of a large sample of cluster radio sources. We compute fractional univariate and bivariate RLF, in which the normalisation makes use of the number of cD, D, E and S0 galaxies in the 41 clusters that were surveyed completely out to $r/R_{\rm A} = 0{\cdot}24$. We use the results of Ledlow and Owen, who analysed the photographic data of

Dressler (1980), to determine the number of early-type galaxies in 25 clusters. Using their analysis, we conclude that each cluster contains an average of 10 galaxies with absolute luminosities in the range $-21{\cdot}0 \geq M_{\rm R} \geq -25{\cdot}0$, which is the luminosity range covered by our cluster identifications. When the fractional RLF is normalised in this way, we obtain the probability of an early-type cluster galaxy being a radio source above the detection limit of the survey.

An allowance is made for the incompleteness of the survey at the lowest radio powers; for example, in the lowest power bin with mid-power $10^{22{\cdot}1}$ W Hz^{-1}, only 11 of the 36 clusters can be considered as completely surveyed. The number of completely surveyed clusters reaches the maximum of 41 for mid-power $\geq 10^{23{\cdot}3}$ W Hz^{-1}.

Despite the fact that our sample of radio galaxies is not complete to a given redshift, a comparison of Fig. 9 (this paper) with Fig. 3 of Ledlow and Owen (1996) shows that both sets of data occupy very similar regions in radio power–optical power space. On this basis, we suggest that it is legitimate to compare the RLF from the two sets of data.

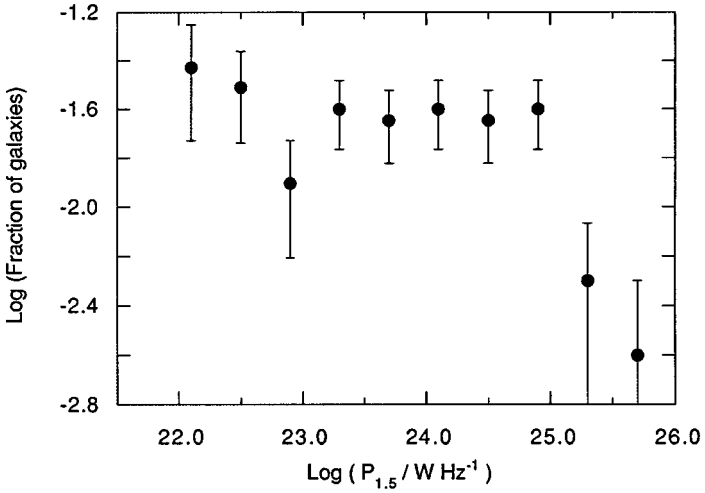

Fig. 17. Fractional univariate luminosity function from the completely surveyed sample out to $r/R_{\rm A} = 0{\cdot}23$. The sampling errors are proportional to $\pm\sqrt{N}$.

Fig. 17 shows the univariate FRLF derived from our data. It is similar to that presented by Ledlow and Owen in their Fig. 6. The probability of an early-type cluster galaxy being detected remains relatively constant at $\sim 0{\cdot}02$ for radio powers $10^{22{\cdot}1} \leq P_{1{\cdot}5} \leq 10^{24{\cdot}9}$ W Hz^{-1}. The detection probability then drops rapidly by a factor of $\sim$6 for the power range $10^{25{\cdot}3} \leq P_{1{\cdot}5} \leq 10^{25{\cdot}7}$ W Hz^{-1}, although the errors are large in this region because of the small numbers of sources.

Fig. 18 shows the integral bivariate FRLF with bin sizes of 1 mag in $M_{\rm R}$ and $0{\cdot}75$ in $\log(P_{1{\cdot}5}/{\rm W\ Hz^{-1}})$. This figure clarifies the partial correlation between $\log P_{1{\cdot}5}$ and $\log P_{\rm R}$ seen in Fig. 9. The probability of detecting a radio source increases markedly with absolute brightness for all radio powers, although the

probability drops continuously with radio power in each bin of absolute magnitude. This luminosity function is similar to Fig. 8 of Ledlow and Owen (1996), but our respective FRLF differ in the slope; we derive a flatter FRLF, implying that a larger fraction of the more powerful radio sources in our sample is associated with cluster galaxies.

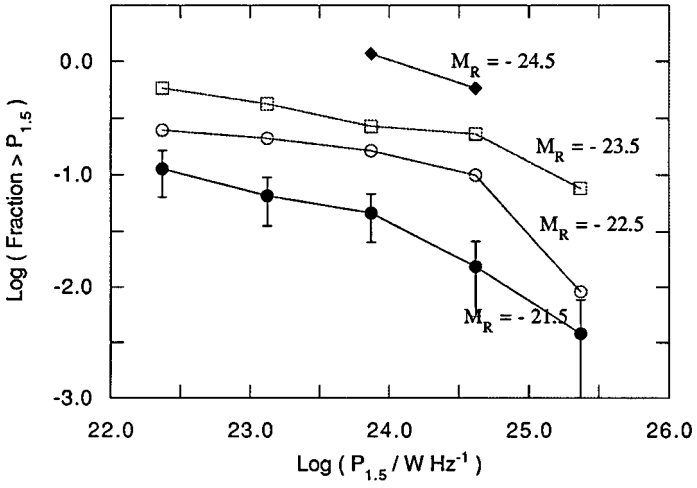

Fig. 18. Integrated fractional bivariate luminosity function from the completely surveyed sample out to $r/R_{\rm A} = 0{\cdot}23$. The sampling errors are proportional to $\pm\sqrt{N}$, but are provided for only one magnitude bin to avoid confusion.

8. Confinement and Age of the Cluster Sources

Our angular resolution is insufficient to resolve the jets, so that our observations constrain mainly the age and confinement of the lobes in radio galaxies; even when the source cannot be resolved, one can assume the presence of lobes in most sources. We shall confine our attention to the sources in Table 4 with measured or implied redshifts and, consequently, estimates of linear size, surface brightness and $B_{\rm me}$, which we have already shown in Section 6*a* to vary systematically between the three polarisation classes; such a procedure enables us to investigate the confinement and age over wide ranges of intrinsic source parameters.

(8a) Computational Method

We use equations (6), (7) and (8) in Section 3·1 of Miley (1980) to estimate travel-time from an assumed once-only acceleration site in the nucleus or inner jets of the host galaxy, using the present observed linear projected distance of the radio lobe's centroid from the acceleration site and an assumed constant velocity of outflow. If the assumptions are correct, then the synchrotron+inverse-Compton aging time as computed from equation (7) of Section 3·1·4 in Miley (1980) should approximately equal the travel time. The aging time requires information about a 'break' in the radio spectrum at a frequency above which the spectrum steepens exponentially. The spectra are reasonably well known for only some of the cluster sources in our sample, partly from the present VLA study and partly

from the more extensive detailed spectra of the stronger sources published in Slee and Siegman (1983). A spectral break in sources of polarisation Classes I and II must lie above 4·9 GHz, since we see no evidence in these spectra for the break below 4·9 GHz. Some of the sources in Class III (e.g. A115__2a/b and A2052__1) show evidence for a break above 1·5 GHz. Here, we shall adopt a break above 4·9 GHz to calculate an upper limit to source age, although its exact value affects the derived age by only the square root.

(8b) Representative Travel-times and Ages

To obtain travel-times and ages for sources with a wide range of intrinsic parameters, we have used the median values for the three polarisation classes shown in Table 4 (using only the sources with measured or inferred redshifts). Adopting a bulk plasma speed of 1000 km s^{-1} (of the order of the sound speed), we find that the travel times decrease from $3{\cdot}7\times10^7$ yr in Class I to $6{\cdot}2\times10^6$ yr in Class III (mainly because the angular distances from the galaxies to the lobe centroids decrease by a similar factor). The upper limit to the age inferred from the spectral break at >4·9 GHz is $<1{\cdot}2\times10^7$ yr in Class I and $<2{\cdot}8\times10^6$ yr in Class III (because their $B_{\rm me}$ increase by a factor of 3·3 over the same classes). The ratio of travel time to age remains fairly constant at ∼3, although the ratio should be ≤1 if there is only one initial acceleration site at the centre of the host galaxy. This is not a serious disagreement since the travel time can easily be reduced by this factor by increasing the bulk speed to ≥3000 km s^{-1}, which is consistent with the bulk speeds of 4500–5500 km s^{-1} proposed by Andernach *et al.* (1992) in a study of the radio galaxies 3C31 and 3C449. A similar agreement could be reached by allowing the field to fall below the minimum energy values by a factor of three, although we have already cited evidence in Section 6 for the validity of the equipartition argument and the value of $B_{\rm me}$ derived from it. There is thus no clear evidence from these data that continuing re-acceleration is required to maintain cluster radio galaxies.

We note that, recently, some authors have questioned the validity of the assumptions in the simple model used above, and they claim that the ages of radio galaxies are at least a factor of 10 higher than calculated on the basis of that model. Their reasons are derived from the observation that radio lobes under high angular resolution usually show regions of enhanced surface brightness, implying the presence of *in situ* acceleration sites (e.g. Eilek 1996). It is claimed that, despite the cessation of particle injection from the inner jets, a spectral break will still appear in the lobe spectrum at a frequency determined by equilibrium between the competing processes of synchrotron aging and electron re-acceleration. It follows that, if the lobe age is higher by a large factor than in the simple model used here, then our computations of plasma bulk speed need to be completely revised (probably upwards) to account for the possible generation of shock waves to generate the re-acceleration process.

(8c) Confinement of Cluster Radio Galaxies

The most likely confinement mechanisms are the pressure exerted on the radio plasma by the hot intra-cluster gas and/or the dynamic ram pressure caused by the motion of the source through the intra-cluster gas. Since most of the sources are within 300 kpc of the cluster centre (see Fig. 5), where $T_{\rm e} \sim 10^8$

K and $10^{-3} \leq n_e \leq 10^{-2}\,\mathrm{cm}^{-3}$, these mechanisms are likely to be particularly effective. We consider the two confinement mechanisms below with the help of the inequalities in Table 1 of Section 3.1.2 in Miley (1980):

(i) *Static thermal pressure*. We evaluated the equation for the three polarisation classes, each of which has significantly different values of B_{me}. The static thermal pressure is able to confine the radio lobes with intra-cluster electron density as low as $10^{-4}\,\mathrm{cm}^{-3}$ in Class I lobes and $10^{-3}\,\mathrm{cm}^{-3}$ in Class III lobes.

(ii) *Ram pressure*. We evaluated the equation for a translational velocity of $1000\,\mathrm{km\,s}^{-1}$ for the host galaxy, and $n_e = 10^{-3}\,\mathrm{cm}^{-3}$. The confinement inequality was satisfied for Class I and II lobes but not for Class III. However, we know that the restriction of Class III sources to the very centre of the cluster will ensure confinement by static thermal pressure alone.

In summary, it is clear that both confinement mechanisms are operating on the lobes of cluster radio galaxies. The static pressure model is generally applicable, but the ram-pressure mechanism would also be effective on radio galaxies with translational velocities $\geq$1000 $\mathrm{km\,s}^{-1}$. There seems to be no problem in confining the radio lobes by the intra-cluster gas, in agreement with the independent study of Morganti *et al.* (1988).

9. Relation between Optical, Radio and X-ray Luminosities

We have already shown in Paper II that there is a significant positive correlation between radio power and X-ray luminosity in clusters. In that analysis we included all radio sources with $r/R_A \leq 0{\cdot}28$, regardless of whether or not they had been identified with cluster galaxies. In this analysis, we include only identified cluster sources from clusters that had been surveyed completely out to either $r/R_A \leq 0{\cdot}24$ or $\leq 0{\cdot}51$, i.e. the two samples first defined in Section 2*d* and subsequently used for most numerical analyses. ROSAT luminosities are available for 22 clusters in the first sample and 11 clusters in the second sample. We shall concentrate on the bigger sample of 22 clusters surveyed out to $r/R_A \leq 0{\cdot}24$, but will seek confirmation from the smaller sample of 11 clusters surveyed out to $r/R_A \leq 0{\cdot}51$. There are three (not necessarily independent) correlations to consider:

(i) *Radio power versus X-ray luminosity*. We summed the radio powers of identified sources with $r/R_A \leq 0{\cdot}24$ and plotted them against the corresponding ROSAT luminosities taken mainly from Ebeling *et al.* (1996). The scatter diagram is shown in Fig. 19; the regression line has a slope of $+0{\cdot}73$ and the correlation is significant at the 4% level. This confirms the relationship shown in Fig. 5 of Paper II, although the slopes are rather different. The smaller sample of clusters with X-ray luminosities surveyed completely out to $r/R_A \leq 0{\cdot}51$ confirms the trend of Fig. 16, but the correlation is significant at only the 9% level.

(ii) *Optical luminosity versus X-ray luminosity*. We summed the optical luminosities of the galaxies identified with radio sources with $r/R_A \leq 0{\cdot}24$ and plotted them against the corresponding ROSAT luminosities. The scatter diagram is shown in Fig. 20; the regression line has a slope of $+1{\cdot}31$ and the correlation is significant at the $<0{\cdot}5$% level. A similar plot was obtained for the smaller sample out to $r/R_A \leq 0{\cdot}51$ with a slope of $+0{\cdot}61$ and a significance level of $2{\cdot}5$%. In this analysis, we have not included the numerous cluster galaxies with

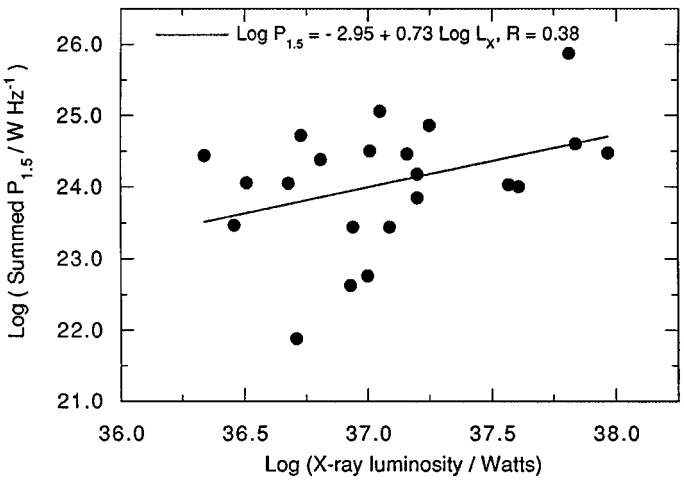

Fig. 19. Correlation between summed radio power and cluster X-ray luminosity in the completely surveyed sample out to $r/R_{\rm A} = 0{\cdot}23$. The regression line and its equation are shown. The correlation is significant at $P = 0{\cdot}04$.

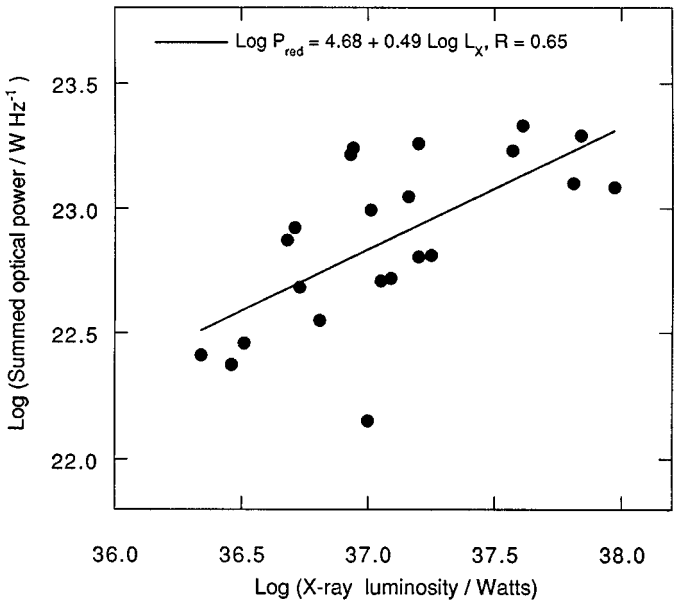

Fig. 20. Correlation between summed red optical power of cluster galaxies that are associated with radio sources and cluster X-ray luminosity in the completely surveyed sample out to $r/R_{\rm A} = 0{\cdot}23$. The regression line and its equation are shown. The correlation is significant at $P < 0{\cdot}005$.

no detectable radio emission. Such galaxies are usually at least 3 magnitudes fainter than those of the radio identifications and, individually, contribute little to the optical power; for example, in Abell 85, 40 galaxies with $M_{\rm R} = -20{\cdot}0$ would contribute only the same total optical power as the central cD.

(iii) *Radio power versus optical luminosity*. We plotted the summed radio powers out to $r/R_A \leq 0{\cdot}24$ against the corresponding summed optical luminosities. The trend was for a positive correlation, although the significance was low at $>0{\cdot}10$. This was confirmed by the sample out to $r/R_A = 0{\cdot}51$.

We then applied corrections for Malmquist bias as explained in Section 5 in connection with the regression analysis of the parameters in Table 4. In the summed radio power versus X-ray luminosity regression, the slope was reduced from $0{\cdot}73$ to $0{\cdot}54$, but the correlation coefficient was unaffected. In the summed optical power versus X-ray luminosity regression, the slope was reduced from $0{\cdot}49$ to $0{\cdot}36$ and the correlation coefficient fell from $0{\cdot}65$ to $0{\cdot}59$; this is still a highly significant regression.

Although we have confirmed the correlation between radio power and X-ray luminosity found in Paper II, the more outstanding relationship is the positive correlation between optical and X-ray luminosity. At first glance, the lack of a strong correlation between radio power and optical luminosity is not consistent with the very significant correlation mentioned in Section 5, but the latter was obtained from many more identified radio sources (65 sources versus 22 summed powers from clusters with X-ray data). The lack of a strong relationship in item (iii) above does, however, indicate that the two significant relationships in items (i) and (ii) are independent.

On the optical versus X-ray correlation, it appears that either the luminosities of the cluster galaxies that are hosts of radio sources are influenced by the density and temperature of the hot intra-cluster gas (perhaps by causing more galaxy mergers) or that the properties of the hot gas depend on the host's luminosity (perhaps by outflow of gas). It is, of course, possible that both processes are operating.

On the radio versus X-ray correlation, the comparatively short lifetimes of radio galaxies ensures that it is the long-lived, hot intra-cluster gas that has affected the radio power, probably by preventing the adiabatic expansion of the source.

10. Cores and Inner Jets of Cluster Galaxies

We reported in Paper II measurements on the stronger sources in southern clusters with the Parkes–Tidbinbilla Interferometer (PTI). The observations were made at $8{\cdot}4$ GHz with a fringe spacing of $\sim$27 milliarcsec, sufficient to resolve out the lobes and yield the flux density in the core and inner jets. These core flux densities are listed in Table 2 of Paper II. We combine these measurements with PTI measurements of a complete sample of FR I radio galaxies that have a similar distribution of total radio powers (Slee *et al.* 1994*b*); the latter sample contains 22 and 62 identified radio sources (with measured redshifts) that are respectively in and outside Abell clusters.

The $8{\cdot}4$-GHz core flux densities of the present VLA cluster sample were transformed to 5-GHz flux densities by using the median core spectral index of $+0{\cdot}28$, found by Slee *et al.* (1994*b*). This transformation to a frequency at which most other published core measurements have been made facilitates the comparison between the cluster and non-cluster samples. The resulting 5-GHz core flux densities were then converted to 5-GHz core powers by means of the cluster redshifts. Remember that only 27% of the identifications in the present

VLA sample had redshift measurements; the rest were allocated to clusters from considerations of absolute red luminosity, as outlined in Section 2*d*.

The present VLA cluster sample consists of 33 sources, in which only four cores were detected with the PTI. A much larger fraction of the sample of Slee *et al.* (1994*b*), in both the cluster and non-cluster categories, was detected. The discrepancy is probably because of the generally higher redshift range of the VLA sample. We have added the VLA cluster sample to the subset of cluster sources from Slee *et al.* (1994*b*), and tested the two distributions of core flux density (including upper limits for the undetected sources) for significant differences. The analysis was done with the ASURV (UNIVAR) package of Feigelson and Nelson (1985). There were 62 measurements made in the non-cluster group and 53 in the cluster sample.

The result showed that the core power distributions were consistent with having been drawn from the same parent population. There is no evidence that the core power of cluster and non-cluster radio galaxies with similar distributions of total power differ systematically. This is an interesting result in that it shows that the hot intra-cluster gas near the cluster centre does not provide an extra supply of fuel for the engine at the centre of the galaxy. In addition, the higher confining pressure of the intra-cluster gas does not affect the radio output of the engine.

11. Summary and Conclusions

We have examined a sample of 765 radio sources from a VLA survey at two frequencies of 60 fields near 58 Abell clusters. The observational method and resulting data were published by Slee *et al.* (1989, 1994*a*, 1996). We have devoted considerable attention to the selection of complete flux-limited samples, from which we draw the following conclusions:

(i) The sample is complete for sources within the FWHP primary beam of the VLA with $S_{1\cdot5} \geq 2\cdot0$ mJy.

(ii) The fraction of sources identified with galaxies rises from ∼28% at the lowest flux densities to ∼80% at the high flux-density end of the distribution.

(iii) About 7% of the sample is identified with star-like (St) images. This is twice the chance expectation, suggesting that half of them are QSOs.

(iv) We define two samples of identified cluster radio galaxies, drawn from clusters surveyed completely out to $0\cdot24$ and $0\cdot51$ Abell radii, respectively. About 60% of the sources in these areas are background objects.

(v) The sources in these two samples are strongly concentrated towards their cluster centres with their surface density varying as $(r/R_{\rm A})^{-1\cdot6}$. On average, we detect about two member radio galaxies per cluster with flux density $S_{1\cdot5} \geq 2$ mJy.

(vi) The median values of the redshift-independent parameters of double radio galaxies (i.e. the component ratios of power, projected area and surface brightness) drawn from the complete sample in (i) above were significantly different for cluster and background doubles only in their ratios of projected areas. At the 2% level of significance, the stronger (a) component in a cluster double occupies a larger area than that in a background double. In the rest frame of the cluster doubles, the a component has the larger area, but only with marginal significance ($P = 0\cdot09$). There is no significant difference between the components in surface brightness in the rest frames of cluster doubles.

(vii) The lobes of cluster doubles have spectra that steepen with their radio power ($P = 0{\cdot}006$), and their spectra also steepen with surface brightness, although with less significance ($P = 0{\cdot}1$). This behaviour is the opposite to that found in double-lobed quasars.

(viii) Three of the four significant correlations between intrinsic parameters for the two completely surveyed samples in (iv) above are probably expected (see Figs 8 to 11). The correlation between absolute red magnitude and $r/R_{\rm A}$ is in the sense that the brightest galaxies tend to be nearer the cluster centre; this is certainly not unexpected, but we suggest that the relationship has not hitherto been demonstrated convincingly.

(ix) In the three classes of polarisation data, which we defined as Classes I, II and III, depending on whether polarisation was measurable, respectively, at both frequencies, at the higher frequency only, or at neither, the median source area decreases by a factor of $8{\cdot}5$ from Class I to Class III, the median surface brightness increases by a factor of 9 and the median minimum energy field increases by a factor of $3{\cdot}3$; Class III cluster sources are confined very closely to cluster centres, and are identified with the intrinsically brightest galaxies (Table 4).

(x) The depolarisation in radio lobes is predominantly caused by tangled magnetic fields in Class I and to the combined effects of tangled fields and differential Faraday rotation in Classes II and III. The rms scale size of tangled fields is $\sim$5 kpc, considerably less than the linear beam diameter at the source, accounting for the low polarised fractions detected at $4{\cdot}9$ GHz in Class I and II sources.

(xi) A study of the E-vectors in the lobes of Class I doubles shows that the field directions are predominantly parallel to the double's axis.

(xii) The univariate fractional luminosity function for the completely surveyed sample out to $r/R_{\rm A} = 0{\cdot}24$ (Fig. 17) shows that early-type cluster galaxies with $M_{\rm R} \leq -21{\cdot}0$ have a probability of $\sim 0{\cdot}02$ of being detected as a radio source with $P_{1{\cdot}5} \leq 10^{24{\cdot}9}$ W Hz^{-1}. Higher power radio sources are much less frequently associated with cluster galaxies.

(xiii) The integrated bivariate fractional luminosity function (Fig. 18) shows that cluster radio sources systematically originate in the higher luminosity galaxies over the complete range of radio powers.

(xiv) The lifetimes of cluster radio galaxies depend mainly on the magnetic field strength in their lobes and on any re-acceleration processes that may be present. Lifetimes were found to vary from $<1{\cdot}2{\times}10^7$ yr in polarisation Class I lobes to $<2{\cdot}8{\times}10^6$ yr in Class III sources.

(xv) Relativistic plasma ejected from a single acceleration site at the host galaxy with average speed $\geq$3000 km s^{-1} would account for the estimated source ages in (xiv).

(xvi) The confinement of the lobes can easily be accomplished by the static pressure exerted by the intra-cluster gas, aided by the ram pressure generated by the passage of the galaxy through that medium.

(xvii) The summed radio power from the cluster sources is correlated with the ROSAT X-ray luminosity at the 4% level of significance. There is a somewhat stronger correlation (significance level of $2{\cdot}5\%$) between the summed red absolute magnitude and the X-ray luminosity. Since the correlation between radio and optical luminosities is quite weak in the small (22 clusters) sample with X-ray

data, we suggest that the two significant correlations noted above are independent. Since the lifetimes of radio galaxies are relatively short compared to the lifetime of a cluster, it appears that the radio versus X-ray correlation is caused by the retardation of the adiabatic expansion of the radio source by the strong pressure of the hot intra-cluster gas. On the other hand, it is not clear which is the independent variable in the optical versus X-ray correlation.

(xviii) Our measurements of core power in cluster radio galaxies are consistent with those in non-cluster sources from a complete, independent sample. It appears that the high density of hot gas near a cluster centre does not provide an extra supply of fuel to the nuclear engine.

Acknowledgments

The referee's careful and critical reading of the manuscript has provided many useful improvements to the content of the paper. We thank Dr J. E. Reynolds and Dr G. S. Tsarevsky for their constructive comments. H.A. benefited from financial support by CONACYT (Mexico; Cátedra Patrimonial, ref 950093).

References

Abell, G. O. (1958). *Astrophys. J. Suppl. Ser.* **3**, 211.
Abell, G. O., Corwin, H. G., and Olowin, R. P. (1989). *Astrophys. J. Suppl. Ser.* **70**, 1.
Andernach, H., and Andreazza, C. M. (1990). *Rev. Mexicana Astron. Astrof.* **21**, 136.
Andernach, H., Feretti, L., Giovannini, G., Klein, U., Rossetti, E., and Schnaubelt, J. (1992). *Astron. Astrophys. Suppl. Ser.* **93**, 331.
Andernach, H., Han Tie, Sievers, A., Reuter, H.-P., Junkes, N., and Wielebinski, R. (1988). *Astron. Astrophys. Suppl. Ser.* **73**, 265.
Bahcall, J. N., and Soneira, M. (1980). *Astrophys. J. Suppl. Ser.* **44**, 73.
Burn, B. J. (1966). *Mon. Not. R. Astron. Soc.* **133**, 67.
Cioffi, D. F., and Jones, T. W. (1980). *Astron. J.* **85**, 368.
Dennett-Thorpe, J., Bridle, A. H., Scheuer, P. A. G., Laing, R. A., and Leahy, J. P. (1997). *Mon. Not. R. Astron. Soc.* **289**, 753.
Dressler, A. (1980). *Astrophys. J. Suppl. Ser.* **42**. 565.
Ebeling, H., Voges, W., Böhringer, H., Edge, A. C., Huchra, J. P., and Briel, U. G. (1996). *Mon. Not. R. Astron. Soc.* **281**, 799.
Eilek, J. A. (1996). *ASP Conference Ser.* **100**, 281.
Fabian, A. C. (1994). *Annu. Rev. Astron. Astrophys.* **32**, 277.
Feigelson, E. D., and Nelson, P. I. (1985). *Astrophys. J.* **293**, 192.
Feretti, L., Perola, G. C., and Fanti, R. (1992). *Astron. Astrophys.* **265**, 9.
Fomalont, E. B., and Rogstad, D. H. (1966). *Astrophys. J.* **146**, 528.
Garrington, S. T., and Conway, R. G. (1991). *Mon. Not. R. Astron. Soc.* **250**, 198.
Garrington, S. T., Conway, R. G., and Leahy, J. P. (1991). *Mon. Not. R. Astron. Soc.* **250**, 171.
Ge Jingping, and Owen, F. N. (1994). *Astron. J.* **108**, 1523.
Jaffe, W. J., and Perola, G. C. (1975). *Astron. Astrophys. Suppl. Ser.* **21**, 137.
Kim, K.-T., Tribble, P. C., and Kronberg, P. P. (1991). *Astrophys. J.* **379**, 80.
Kron, R. G., Koo, D. C., and Windhorst, R. A. (1985). *Astron. Astrophys.* **146**, 38.
Ledlow, M. J., and Owen, F. N. (1995*a*). *Astron. J.* **109**, 853.
Ledlow, M. J., and Owen, F. N. (1995*b*). *Astron. J.* **110**, 1959.
Ledlow, M. J., and Owen, F. N. (1996). *Astron. J.* **112**, 9.
McHardy, I. M. (1978). *Mon. Not. R. Astron. Soc.* **185**, 927.
McHardy, I. M. (1979). *Mon. Not. R. Astron. Soc.* **188**, 495.
Miley, G. (1980). *Ann. Rev. Astron. Astrophys.* **18**, 165.
Mills, B. Y., and Hoskins, D. G. (1977). *Aust. J. Phys.* **30**, 509.
Morganti, R., Fanti, R., Gioia, I. M., Harris, D. E., Parma, P., and de Ruiter, H. (1988). *Astron. Astrophys.* **189**, 11.

Morganti, R., Parma, P., Capetti, A., Fanti, R., de Ruiter, H. R., and Prandoni, L. (1997). *Astron. Astrophys. Suppl. Ser.* **126**, 335.
Owen, F. N., White, R. A., Hilldrup, K. C., and Hanisch, R. J. (1982). *Astron. J.* **87**, 1083.
Pacholczyk, A. G. (1970). *In* 'Radio Astrophysics' (Freeman: San Francisco).
Perley, R. A. (1982). *Astron. J.* **87**, 859.
Pislar, V., Durret, F., Gerbal, D., Lima Neto, G. B., and Slezak, E. (1997). *Astron. Astrophys.* **322**, 53.
Reynolds, J. E. (1986). Ph.D. thesis, University of Sydney.
Riley, J. M. (1975). *Mon. Not. R. Astron. Soc.* **170**, 53.
Robertson, J. G., and Roach, G. J. (1990). *Mon. Not. R. Astron. Soc.* **247**, 387.
Ryan, S. G. (1989). *Astron. J.* **98**. 1693.
Sadler, E. M., Jenkins, C. R., and Kotanyi, C. G. (1989). *Mon. Not. R. Astron. Soc.* **240**, 591.
Slee, O. B., and Siegman, B. C. (1983). *Proc. Aston. Soc. Aust.* **5**, 114.
Slee, O. B., Wilson, I. R. G., and Siegman, B. C. (1983). *Aust. J. Phys.* **36**, 101.
Slee, O. B., Perley, R. A., and Siegman, B. C. (1989). *Aust. J. Phys.* **42**, 633 (Paper I).
Slee, O. B., Roy, A. L., and Savage, A. (1994*a*). *Aust. J. Phys.* **47**, 145 (Paper II).
Slee, O. B., Sadler, E. M., Reynolds, J. E., and Ekers, R. D. (1994*b*). *Mon. Not. R. Astron. Soc.* **269**, 928.
Slee, O. B., Roy, A. L., and Andernach, H. (1996). *Aust. J. Phys.* **49**, 977 (Paper III).
Slingo, A. (1974*a*). *Mon. Not. R. Astron. Soc.* **166**, 101.
Slingo, A. (1974*b*). *Mon. Not. R. Astron. Soc.* **168**, 307.
Tyson, J. A., and Jarvis, J. F. (1979). *Astrophys. J.* **230**, L153.
Verter, F. (1993). *Astrophys. J.* **402**, 141.
Wall, J. V. (1994). *Aust. J. Phys.* **47**, 625.
Windhorst, R. A., Miley, G. K., Owen, F. N., Kron, R. G., and Koo, D. C. (1985). *Astrophys. J.* **289**, 494.

Manuscript received 8 December 1997, accepted 20 August 1998